Necdin shapes serotonergic development and SERT activity modulating breathing in a mouse model for Prader-Willi Syndrome.

Valéry Matarazzo[1#], Laura Caccialupi[1*], Fabienne Schaller[1*], Yuri Shvarev[2*], Nazim Kourdougli[1], Alessandra Bertoni[1], Clément Menuet[1], Nicolas Voituron[3], Evan Deneris[4], Patricia Gaspar[5], Laurent Bezin[6], Pascale Durbec[7], Gérard Hilaire[1], Françoise Muscatelli[1#]

[1] Aix Marseille Univ, INSERM, INMED, Marseille, France
[2] Department of Women's and Children's Health, Karolinska Institute, Solna, Sweden
[3] Université Paris 13, UFR STAPS, Paris, France
[4] Department of Neurosciences, Case Western Reserve University, Cleveland, OH, USA
[5] UPMC Univ Paris 6, Institut du Fer à Moulin, INSERM, Paris, France
[6] Université de Lyon, INSERM, CNRS, Lyon Neuroscience Research Center, Lyon, France
[7] Aix Marseille Univ, CNRS, IBDM, Marseille, France

*: equal contribution
#: corresponding authors
Emails: valery.matarazzo@inserm.fr; francoise.muscatelli@inserm.fr.
Institut de Neurobiologie de la Méditerranée (INMED)
INSERM-Aix Marseille Université, UMR901
Campus Scientifique de Luminy, 13273 Marseille, France

Number of pages: 35

Number of words: 3198 (including references)

Number of figures: 4 figures /9 supplement figures / 2 supplement movies / 3 data source files.

Keywords: respiration, apnea, raphe nucleus, SSRI, Serotonin transporter.

ABSTRACT

Prader-Willi syndrome (PWS) is a genetic neurodevelopmental disorder that presents with hypotonia and respiratory distress in neonates. The *Necdin*-deficient mouse is the only model that reproduces the respiratory phenotype of PWS (central apnea and blunted response to respiratory challenges). Here, we report that *Necdin* deletion disturbs the migration of serotonin (5-HT) neuronal precursors, leading to altered global serotonergic neuroarchitecture and increased spontaneous firing of 5-HT neurons. We show an increased expression and activity of 5-HT Transporter (SERT/Slc6a4) in 5-HT neurons leading to an increase of 5-HT uptake. In *Necdin*-KO pups, the genetic deletion of *Slc6a4* or treatment with Fluoxetine, a 5-HT reuptake inhibitor, restored normal breathing. Unexpectedly, Fluoxetine administration was associated with respiratory side effects in wild-type animals. Overall, our results demonstrate that an increase of SERT activity is sufficient to cause the apneas in *Necdin*-KO pups, and that Fluoxetine may offer therapeutic benefits to PWS patients with respiratory complications.

INTRODUCTION

Respiration is a complex function controlled in large part by raphe serotonergic (5-HT) neurons (Teran et al., 2014). Central 5-HT depletion induces severe apneas during the early postnatal period (Barrett et al., 2016; Trowbridge et al., 2011) and serotonopathy is implicated in the genesis of breathing disorders in human pathologies including neurodevelopmental diseases such as Sudden Infant Death Syndrome (Duncan et al., 2010; Hilaire et al., 2010; Kinney et al., 2011; Paterson et al., 2009), Rett syndrome (Abdala et al., 2010; Toward et al., 2013) and Prader-Willi Syndrome (PWS) (Zanella et al., 2008). However, the cellular and molecular events that underlie serotonopathy, and the causal link between serotonopathy and respiratory dysfunction in these pathologies are poorly understood.

PWS (prevalence 1/20000) is characterized by a combination of endocrine, metabolic, cognitive and behavioural/psychiatric symptoms (OMIM #176270). Its associated respiratory disturbances (J. Miller et al., 2013; Nixon et al., 2002; Tan et al., 2017) are highly disruptive to the daily life of patients and represent the most common cause of death (73% of infants and 26% of adults) (Butler et al., 2017). They include both obstructive (Festen et al., 2006; Pavone et al., 2015) and central sleep apneas {Festen, 2006 #1495; Sedky et al., 2014), and blunted responses to hypercapnia/hypoxia possibly due to a lack of chemoreceptor sensitivity (Arens et al., 1996; Gozal et al., 1994; Schluter et al., 1997; Gillett et al., 2016). Central apneas are present at birth (Zanella et al., 2008) and are prevalent throughout infancy while obstructive sleep apneas are more frequent in adolescents (Cohen et al., 2014).

PWS is caused by the loss of paternal expression of several genes of the 15q11-q13 region, including *NECDIN*. Necdin protein is a member of the Mage family, with proposed functions in differentiation (Andrieu et al., 2003; Takazaki et al., 2002), migration (Kuwajima et al., 2010; N. L. Miller et al., 2009; Tennese et al., 2008), neurite growth (Liu et al., 2009; Tennese et al., 2008), axonal extension, arborization and fasciculation (Pagliardini et al., 2005), and cell survival (Aebischer et al., 2011; Andrieu et al., 2006; Kuwako et al., 2005; Tennese et al., 2008). Among several mouse models of PWS, only those with Necdin deletion, *Necdin (Ndn)*-KO mouse models ($Ndn^{tm1\text{-}Stw}$(Gerard et al., 1999) and $Ndn^{tm1\text{-}Mus}$(Muscatelli et al., 2000)), present breathing deficits. Newborns *Ndn*-KO showed severe arhythmia, apnea, and blunted responses to respiratory challenges that frequently result in early postnatal lethality (Ren et al., 2003; Zanella et al., 2008). This dyspnoeic phenotype is recapitulated in brainstem slices that contain the Inspiratory Rhythm Generator (IRG), which display an irregular inspiratory rhythm and apneas (Ren et al., 2003; Zanella et al., 2008). Interestingly, 5-HT application, as well as other neuromodulators that are commonly co-released by medullary 5-HT neurons, such as substance P and thyrotropin-releasing hormone

(Hodges et al., 2008; Holtman et al., 1994; Kachidian et al., 1991; Ptak et al., 2009), stabilized the *in vitro* inspiratory rhythm (Pagliardini et al., 2005; Zanella et al., 2008).

A role for serotonergic transmission in the genesis of respiratory dysfunction in the *Necdin*-KO model is supported by neuroanatomical studies: Pagliardini and colleagues report abnormal morphology and orientation of axonal fibers that contain large 5-HT/Substance P varicosities in the developing $Ndn^{tm1\text{-}Stw}$-KO medulla (Pagliardini et al., 2005; Pagliardini et al., 2008). Similarly, we have also previously found that 5-HT fibers contained "swollen 5-HT varicosities" in the $Ndn^{tm1\text{-}Mus}$-KO model, and that *Necdin* is expressed in virtually all 5-HT neurons (Zanella et al., 2008).

These findings suggest a potential role for abnormalities in 5-HT metabolism and release as a potential mediator of respiratory dysfunction in the *Necdin*-KO model of PWS, but fall short of proving causality. Here we demonstrate a causal link between the perturbed development of the 5-HT system in $Ndn^{tm1\text{-}Mus}$-KO mice (referred to hereafter as *Ndn*-KO) and their observed respiratory phenotype (central apnea and hypercapnia). Our data implicate increased activity of serotonin transporter (SERT) as a key mediator of central apnea in this model, and that its inhibition restores normal breathing in *Ndn*-KO mice.

RESULTS and DISCUSSION

Lack of Necdin affects the development and function of 5-HT neurons

Pet-EYFP mice expressing YFP under Pet1-promoter control, an early marker of developing 5-HT neurons (Hawthorne et al., 2010), were used to show that Necdin is expressed from E10.5 in early post-mitotic 5-HT precursors and later on in all 5-HT neurons until adulthood (Figure 1A-figure supplement 1A-I).

We then assessed whether Necdin deficiency could induce alterations of 5-HT neuronal development. In wild-type mice rostral hindbrain 5-HT neurons project to the mesencephalon

at E12.5, and we observed a decrease in those ascending 5-HT projections in *Ndn*-KO embryos (Figure 1-figure supplement 1J), confirming previous work (Pagliardini et al., 2008). At E16.5, when the 5-HT raphe nuclei reach their mature configuration, we observed misplaced 5-HT neurons in *Ndn*-KO embryos (Figure 1 B), with ~30% reduction in the total number of 5-HT neurons in the B1-B2 caudal raphe nuclei at birth (Figure 1 C).

Our observations suggested a defect in 5-HT neuronal migration; which was tested using the *Pet-EYFP* model. In E10.5 WT embryos, Pet-EYFP neurons displayed typical bipolar morphology with oval-shaped somata aligned with two primitive processes attached to the ventricular and pial surfaces, required for somal translocation and involved in migration processes (Hawthorne et al., 2010) (Figure 1D). In contrast cells were not correctly aligned and process orientation was significantly disturbed in *Pet-EYFP*/*Ndn*-KO embryos (Figure 1D-E). Cell migration was also defective in organotypic slice cultures prepared from E12.5 embryos. Two-photon time-lapse imaging indicated that migratory behavior, based on somal translocation, was altered in *Ndn*-KO mice (Figure 1F-H-supplement movie 1 and 2) with tracked cells exhibiting increased tortuosity (Figure 1G) and decreased velocity (Figure 1H) of their growth trajectories. Interestingly, a comparable migration defect has been described in primary cultures of $Ndn^{tm1\text{-}Stw}$-KO cortical neurons (Bush et al., 2010). Here we revealed an alteration of cell migration of 5-HT precursors leading to misplaced 5-HT raphe nuclei in *Ndn*-KO mice.

The acquisition of specific firing properties is considered a critical marker of 5-HT neuronal and circuit maturation (Rood et al., 2014). Using visually guided patch-clamp recordings on brain slices (P15), we demonstrated a significant increase of spontaneous firing in *Pet-EYFP*/*Ndn*-KO cells (Figure 1I-K) suggesting a decreased availability of extracellular 5-HT (Maejima et al., 2013). Overall, our results show that Necdin is responsible for the normal

132 migration of 5-HT precursor neurons during development and exerts effects on their
133 electrophysiological properties in post-natal life.

134 **Lack of Necdin increases the expression and activity of serotonin transporter**

135 We hypothesised that reduced availability of extracellular 5HT could have contributed to the
136 excessive electrophysiological activity we observed in Pet-EYFP neurons in *Ndn*-KO animals
137 and examined potential mechanisms through which extracellular 5-HT could be reduced. We
138 compared the distributions of 5-HT- immunoreactive enLarged Punctiform Axonal stainings
139 (5-HT LPAs, previously named "swollen large varicosities" (Pagliardini et al., 2005; Zanella
140 et al., 2008)) in *Ndn*-KO and WT mice. In all regions analyzed we found significantly more 5-
141 HT LPAs in *Ndn*-KO mice (Figure 2A-B). These 5-HT LPAs could result from 1) an increase
142 of 5-HT synthesis and/or 2) a decrease in 5-HT degradation and/or 3) an increase of 5-HT
143 reuptake. HPLC analyses showed a similar level of L-Trp and 5-HT in *Ndn*-KO compared
144 with WT mice, but a significant increase of 5HIAA product in mutants (the ratio of 5HIAA/5-
145 HT also being increased: Figure 2-figure supplement 1A-D). Noticeably, transcript levels of
146 Tryptophan hydroxylase 2, the enzyme that converts L-Trp to 5-HT, were similar in *Ndn*-KO
147 and WT mice (Figure 2-supplement 1E). These results suggest that the increase in 5-HT LPAs
148 found in *Ndn*-KO brainstems probably result from an accumulation of intracellular 5-HT due
149 to an increased 5-HT reuptake, since there is no increase of 5-HT synthesis but, on the
150 contrary, an increase of 5-HT degradation.
151 We hypothesised that overexpression of serotonin transporter (SERT) represents a plausible
152 mechanism through which 5-HT could be accumulated in *Ndn*-KO mice, based on the
153 observation that inactivation of *Maged1*, another member of the *Mage* gene family, leads to
154 overexpression of SERT (encoded by the *Slc6a4* gene) (Mouri et al., 2012). Indeed, we
155 observed a 3.2 fold increase in SERT protein expression in the brainstems of *Ndn*-KO
156 compared to WT pups (Figure 2C-D), while *Slc6a4* transcript levels were similar (Figure 2-

figure supplement 1F). This suggests post-transcriptional or post-translational dysregulation of *Slc6a4*/SERT in *Ndn*-KO. Subsequently, in 5-HT neurons of raphe primary cultures, we assessed SERT activity by live single cell uptake assay, using ASP+ (4(4-(dimethylamino)styryl)-N-methylpyridinium), a fluorescent substrate of SERT (Lau et al., 2015; Oz et al., 2010). Changes in the kinetics and saturation of ASP+ uptake were measured after 8 days *in vitro* culture in 5-HT neurons from neonatal (P0) WT, *Ndn*-KO, and *Slc6a4*-KO mice (Figure 2E-H –figure supplement 2A-B). As expected, cultures accumulated ASP+ over time in all conditions tested. However, kinetics experiments show that ASP+ accumulation was significantly faster (greater mean velocity v) in *Ndn-KO* compared to WT raphe neurons (Figure 2E). Saturation experiments using increasing concentrations of ASP+ confirmed that ASP+ uptake is a saturable process (Figure 2F) and showed a Vmax (Figure 2G) and KM (Figure 2H) significantly higher in *Ndn*-KO than in WT or *Slc6a4*-KO neurons. ASP+ uptake was ~2 fold increased in *Ndn*-KO while it was null in *Slc6a4*-KO cell cultures. We conclude that there is an increase of ASP+ uptake in *Ndn*-KO neurons, specifically dependent on SERT activity, suggesting a mechanism for 5-HT LPAs accumulation *in vivo*. To determine whether *in vivo* deletion of *Slc6a4* could suppress the 5-HT LPAs in *Ndn*-KO, we compared the number of 5-HT LPAs in *Ndn*-KO, *Slc6a4*-KO and *Ndn*/*Slc6a4*-double KO (*Ndn*/*Slc6a4*-DKO) neonates in various brain structures. The number of 5-HT LPAs was similar in brains of *Ndn*/*Slc6a4*-DKO and WT mice (Figure 2A-B), indicating that the absence of *Ndn* is functionally compensated for by the lack of *Slc6a4*.

Together, our data show that increased SERT expression in *Ndn*-KO mice underlies an increase of 5-HT reuptake, which accumulates in 5-HT LPAs. In the absence of any increase in 5-HT synthesis (and in fact increased 5-HT degradation), this sequence of events could be sufficient to cause a physiologically relevant decrease extracellular 5-HT.

Genetic ablation or pharmacological inhibition of SERT uptake restores normal breathing in *Ndn*-KO mice

As exogenous 5-HT application stabilized respiratory rhythm of *Ndn*-KO mice *in vitro,* (Zanella et al., 2008), we hypothesized that SERT dysregulation observed in *Ndn*-KO mice might underlie their respiratory phenotype. To further investigate this causal link we compared breathing parameters in WT, *Ndn*-KO, *Ndn*/ *Slc6a4*-DKO and in *Ndn*-KO pups treated with Fluoxetine, a selective 5-HT reuptake inhibitor (SSRI) used clinically to increase extracellular 5-HT (Figure 3A-B). First, we confirmed that respiratory deficits, quantified as the percentage of mice exhibiting apnea (Figure 3C), the number of apneas per hour (Figure 3D), or the accumulated apnea duration (Figure 3E), were significantly increased in *Ndn*-KO compared to WT mice. These deficits were suppressed by reducing SERT function either by constitutive genetic inactivation (*Ndn*/*Slc6a4*-DKO pups) or by 10 days of Fluoxetine treatment (P5-P15; 10 mg/kg/day) in *Ndn*-KO pups (Figure 3C-E). Other basic respiratory parameters (minute ventilation, frequency of breathing, tidal volume) were unchanged between all genotypes (Figure 3F-H). Therefore, our results show that increasing extracellular 5-HT is sufficient to suppress apneas in juvenile *Ndn*-KO mice.

Since Fluoxetine treatment in early life has positive effects on apneas, we next questioned the long-term consequences of this treatment. Novel cohorts of WT, *Ndn*-KO and *Ndn*-KO pups were treated as above with Fluoxetine or vehicle and then submitted to plethysmography 0, 15 and 45 days after treatment (DAT) (Figure 3-figure supplement 1A-B). The positive effect of Fluoxetine on respiratory function in *Ndn*-KO pups at the end of treatment were confirmed in this cohort, but did not persist at 15 and 45 DAT (Figure 3 –figure supplement 1C-E). Other respiratory parameters (minute ventilation, frequency of breathing, tidal volume) measured at 45 DAT were unchanged between all genotypes (Figure 3 - figure supplement 1F-H).

205 An altered ventilatory response to hypercapnia was previously observed in adult *Ndn*-KO
206 mice (Zanella et al., 2008), so we next investigated whether this deficit is apparent in P0-P1
207 pups. We examined the chemoreflex of *Ndn*-KO and WT neonates by initially subjecting
208 them to a moderate hypercapnia (5 min; 4% CO_2) (Figure 4A–C). Under hypercapnic stress,
209 WT but not *Ndn*-KO neonates progressively increased their respiratory frequency (Rf) (Figure
210 4D), leading to an increase in minute ventilation (volume breathed over 1 min,VE) (Figure
211 4F). In contrast, no significant effects of hypercapnia were detected on any respiratory
212 variables in *Ndn*-KO pups and thus *Ndn*-KO pups appear relatively insensitive to hypercapnia.
213 To determine whether altered central 5-HT transmission contributes to this effect we
214 performed electrophysiological recordings of rhythmic phrenic bursts using *en bloc*
215 brainstem-spinal cord preparations from P0-P1 WT and *Ndn*-KO pups. During perfusion with
216 physiological aCSF (pH 7.4), we found no significant difference in phrenic burst (PB) shape,
217 amplitude or discharge frequency (PBf) between WT and *Ndn*-KO pups (Figure 4G-H). As
218 expected, PBf in WT preparations progressively increased upon acidosis (pH=7.1, Figure 4I,
219 L). However, this effect was not observed in *Ndn*-KO preparations (Figure 4J, L).
220 We then assessed whether increasing extracellular 5-HT could rescue chemoreflex sensitivity
221 in this preparation. Bath application of Fluoxetine (20 μM) prior to acidosis did not affect
222 baseline PBf of *Ndn*-KO preparations (Figure 4K,L), but instead significantly increased PBf
223 responses to acidosis to levels indistinguishable from WT controls (Figure 4K,L).
224 Qualitatively similar responses were observed in experiments in which a 5-HT1A receptor
225 agonist (8OHDPAT) was substituted for Fluoxetine (Figure 4–figure supplement 1A-D). We
226 therefore conclude that the central chemoreceptor hyposensitivity characteristic of the *Ndn*-
227 KO model can be restored by pharmacological manipulations that increase extracellular 5-HT
228 and/or stimulate 5-HT1A-R activity.

Early life Fluoxetine-treatment has deleterious long-term respiratory consequences in WT mice

Although Fluoxetine had beneficial but transient effects on apnea incidence in *Ndn*-KO mice, we observed deleterious and long-lasting effects on respiratory function in WT controls. Early life Fluoxetine-treatment induced a significant increase in the number of apneic mice, the frequency of apneas, and the cumulative distribution of apneas at all timepoints measured (0, 15 and 45 DAT, Figure 3-supplement 2A-E), such that measurements at 45 DAT in WT mice (Figure 3-supplement 2) were similar to those obtained in *Ndn*-KO mice (Figure 3-supplement 1). The sensitivity of WT brainstem-spinal cord preparations, treated with Fluoxetine or with 8OHDPAT, to acute acidosis was similarly affected (Figure 4-figure supplement 2A-D). In neutral aCSF, neither Fluoxetine (Figure 4-figure supplement 2C) or 8OHDPAT (Figure 4-figure supplement 2D) affected resting PBf of WT *en bloc* preparations but instead abolished the normal increases in PBf responses to acidosis. Thus, we confirm that Fluoxetine treatment abolishes the capacity of WT mice to respond to acidosis (Voituron et al., 2010) and we propose a role for 5-HT1A-R activity in this response. We show here, for the first time, adverse effects of Fluoxetine on breathing outcomes.

CONCLUSION

Previously, a pleiotropic function of Necdin has been reported in different neuronal populations and at different developmental stages. Concerning the 5-HT system, an expression of Necdin was observed in virtually all 5-HT neurons (Zanella et al., 2008) and an alteration of the 5-HT system in embryonic and postnatal development was partially described in both *Ndn*-KO (*Ndn*$^{tm1\text{-}Stw}$and *Ndn*$^{tm1\text{-}Mus}$) mouse models, with alterations in 5-HT axonal bundle projections (Lee et al., 2005; Pagliardini et al., 2005) and 5-HT fibers containing swollen 5-HT “varicosities” (Pagliardini et al., 2005; Zanella et al., 2008). Furthermore, an

253 alteration of 5-HT metabolism (Zanella et al., 2008) was observed in mutant neonates
254 suggesting that it might alter 5-HT modulation of the Respiratory Rhythm Generator. Finally,
255 an *in vitro* exogenous application of 5-HT on brainstem-spinal cord preparations of *Ndn*
256 mutant mice alleviates the incidence of apneas (Pagliardini et al., 2005; Zanella et al., 2008).
257 Despite those observations, the pathological mechanism responsible for the serotonopathy in
258 *Ndn*-KO mice and the causal link between this serotonopathy and the breathing alterations
259 were not investigated. Here, we aimed to answer those questions.
260 Noticeably, all previous studies have been performed on heterozygous *Ndn*-deficient mice,
261 with a deletion of the *Ndn* paternal allele only (*Ndn*+m/-p), the maternal allele being normally
262 silent. However we have shown that, due to a faint and variable expression of the *Ndn*
263 maternal allele (+m), *Ndn*+m/-p mice present a variability in the severity of respiratory
264 phenotype compared with the *Ndn*-/- mice (here named *Ndn*-KO) (Rieusset et al., 2013). For
265 instance reduction of 5-HT neurons was not previously found significant in the *Ndn*+m/-p
266 mice (Zanella et al., 2008) but has been found significantly reduced in the *Ndn*-/- mice. In
267 order to avoid such variability and to get consistent results we chose here to study *Ndn*-/-
268 mice.
269 Here, we have shown that Necdin plays a pleiotropic role in the development of 5-HT
270 neuronal precursors that guides the development of central serotonergic circuits and the
271 physiological activity of mature 5-HT neurons. Our results suggest that Necdin controls the
272 level of SERT expression in 5-HT neurons and that lack of Necdin increases the quantity and
273 activity of SERT leading to an increased reuptake and intra-cellular accumulation of 5-HT, as
274 visualized by 5-HT LPAs, leading to a reduction in available extracellular 5-HT. Importantly,
275 *in vivo* inhibition of SERT activity, genetically or pharmacologically (Fluoxetine treatment),
276 is sufficient to prevent the formation of those 5-HT LPAs and suppresses the apnea observed
277 in *Ndn*-KO mice. We also demonstrate, using an *ex vivo* approach, that the altered

chemosensitivity to CO2/acidosis is caused by a central 5-HT deficit and is rescued by Fluoxetine-treatment. We conclude that an increase of 5-HT reuptake is the main cause of breathing deficits (central apnea and hypercapnia response) in *Ndn*-KO mice.

Unexpectedly, we reveal an adverse and long-term effect of early life administration of Fluoxetine on the breathing (apneas, chemosensitivity to CO2/acidosis) of healthy mice. Previous adverse effects have been observed on anxiety and depression (Glover et al., 2016; Millard et al., 2017) after an early postnatal administration of Fluoxetine but the respiratory deficits are reported here for the first time and should be further investigated in another study.

Respiratory failure in patients with PWS constitute a challenging issue since it is the most common cause of death for 73% of infants and 49% of children, (Butler et al., 2017). Death is often linked to respiratory infection or respiratory disorder and may be sudden, with some reported cases of sudden death occurring at night (Gillett and Perez, 2016). In PWS patients, any environmental acute respiratory challenge caused by, for instance, a respiratory tract infection, high altitude or intense physical activity further exacerbates their inherent disability (blunted response to hypoxima/hypercapnia) to adapt an respiratory response. Until now, the underlying pathology for respiratory failure remained elusive and did not appear to be impacted by recent advancements in treatment modalities (Butler et al., 2017). Although oxygen treatment is efficient in preventing the hypoxemia induced by central apneas (Urquhart et al., 2013), such treatment is physically constraining. Within the context of PWS, the current study points towards a critical link between Necdin, serotonopathy, and chemosensing, a function in which brainstem serotonergic circuits play a critical role. Since our study shows that Fluoxetine can suppress apnea and restore chemosensitivity, we propose that Fluoxetine might be an appropriate “acute” treatment that could be considered for Prader-Willi infants/children when they present the first signs of any breathing difficulties.

ACKNOWLEDGMENTS

We thank Camille Dumon and Magdalena Assael for their technical help and the members of the animal facility, genotyping and imaging platforms of INMED laboratory. We thank Pr Keith Dudley for comments and careful reading of the manuscript. Opinions expressed are those of the authors exclusively. This study has been supported by INSERM, CNRS and ANR (Prageder N° ANR-14-CE13-0025-01) grants. Y.S. was supported by Stiftelsen Frimurare Barnhuset i Stockholm grants and N.K.H. Kronprinsessan Lovisas Forening for barnasjukvard; A.B. was supported by FPWR fellowship grant.

MATERIAL AND METHODS

Animals

Mice were handled and cared for in accordance with the Guide for the Care and Use of Laboratory Animals (N.R.C., 1996) and the European Communities Council Directive of September 22th 2010 (2010/63/EU, 74). Experimental protocols were approved by the institutional Ethical Committee guidelines for animal research with the accreditation no. B13-055-19 from the French Ministry of Agriculture. All efforts were made to minimize the number of animals used. Necdin is an imprinted gene, paternally expressed only (Figure 2 supplement 3 and Figure 4 supplement 3). In order to avoid a variability in our results due to a stochastic and faint expression of the maternal allele (Rieusset et al., 2013), we worked with the *Ndn*$^{tm1\text{-}Mus}$ strain and decided to study *Ndn*-/- mice (named here *Ndn*-KO), instead of *Ndn* +m/-p mice as it has been done previously .

Fluoxetine was obtained from Sigma (Saint-Quentin Fallavier, France) for cell culture and *en bloc* medullary experiments and from Mylan pharma for *in vivo* experiments.

Transgenic mice

We bred *ePet-EYFP*-expressing (Scott et al., 2005a; Scott et al., 2005b) or *Slc6a4-Cre* Knock-in (Zhuang et al., 2005) mice with *Ndn*-KO (Muscatelli et al., 2000) mice, all on C57BL/6

328 background. Protocols of genotyping mice have been previously described for *Pet-EYFP*
329 (Hawthorne et al., 2010), *Ndn-KO* (Rieusset et al., 2013) and *Sert*-Cre Knock-in mice
330 (Zhuang et al., 2005), in which the *Slc6a4* gene was replaced by Cre was referred to in the
331 text as *Slc6a4*-KO. Breeding of *Slc6a4*-KO with *Ndn*-KO mice was referred to in the text as
332 *Ndn-Slc6a4*-DKO.

333 **Immunohistochemistry and quantification**

334 Tissue preparation and IHC were performed as previously described (Rieusset et al., 2013).
335 Antibodies used were: rabbit polyclonal anti-Necdin (07-565; Millipore, Bedford, MA, USA;
336 1:500), mouse monoclonal anti-GFP (Interchim, NB600-597; 1:500), goat polyclonal anti-
337 5HT (Immunostar, 20079; 1:300). Sections were examined on a Zeiss Axioplan 2 microscope
338 with an Apotome module.

339 Brainstem structures were sampled by selecting the raphe obscurus area and counting was
340 performed on 3 sagittal sections/animal of 100 µm which represent the entire PET1-YFP
341 positive cell population of the raphe obscurus (ROb/B2) and pallidus (RPa/B1), both nuclei
342 being difficult to separate. For each section, a Z-stack composed of 10 confocal images (8 µm
343 focal spacing) was acquired. For quantification, stereological method has been applied on
344 each Z-stack image using the eCELLence software developed by Glance Vision Technologies
345 (Italy). The total cell number/ per animal was obtained by summing the sub-total of cells
346 counted for the 3 Z-stacks.

347 Images of 5-HT LPAs were acquired using a confocal microscope (Olympus). Between 4 to 8
348 fibers/ brain region for each animal (3WT and 3 KO) were analyzed for the presence of 5-HT
349 LPAs (> 1.8µm^2) on 100 µm long fiber. The size of 5-HT LPAs was quantified using Image J**.**
350 5-HT LPA diameter has been defined *ad arbitrium* as the size of the largest 5-HT punctiform
351 labelling found in the WT fibers.

352 **Organotypic slice cultures and time lapse experiments**

353 Slice cultures from E11.5 embryonic mouse brainstems were prepared from *Pet-EYFP* and
354 *Ndn KO*/*Pet-EYFP* mice. Thick coronal sections (250 µm) brainstem were cut using a tissue
355 chopper and cultured in Neurobasal medium (Thermofisher) containing 2% B27
356 (Thermofisher), 4% horse serum, 10 µg/ml insulin, 200 mM HEPES, 1 % Antibiotic
357 Antimycotic (Thermofisher). For time lapse experiments, the dishes were mounted in a CO_2
358 incubation chamber (5% CO_2 at 37°C) fitted onto an inverted confocal microscope (LSM510,
359 Zeiss). Acquisitions of the region containing raphe Pet-EYFP+ neurons were performed every
360 10 minutes for up to 15 hours. Cell coordinates, velocity, and tortuosity (total length of the
361 track/direct distance from the first to the last point) were calculated using MtrackJ plugin of
362 Image J.

363 **Electrophysiology Patch-clamp**

364 Sagittal slices that included the raphe (400 µm thick) were cut from brainstems of 2 week old
365 *Pet-EYFP* and *Ndn-KO*/*Pet-EYFP* mice. Whole-cell recordings were made from YFP+ cells
366 in the region of the B4 raphe nucleus. During recordings, slices were continuously perfused
367 with artificial cerebrospinal-fluid (aCSF) at 37 °C. Patch pipettes (4-5 MΩ) were filled with
368 an internal solution with the following composition (in mM): 120 KGlu, 10 KCl, 10 Na_2-
369 phosphocreatine, 10 HEPES, 1 $MgCl_2$, 1 EGTA, 2 ATP Na_2, 0.25 GTP Na; pH = 7.3 adjusted
370 with KOH. Current clamp at i=0 were recorded with a HEKA amplifier and acquired using
371 PatchMaster software (HEKA). Offline analysis was performed with Clamfit 10.3.

372 ***In vitro* recordings from *en bloc* brainstem-spinal cord preparations**

373 As previously reported (Berner et al., 2012), the medulla and cervical cord of P0-P1 neonatal
374 mice were dissected, placed in a 2 ml *in vitro* recording chamber, bubbled with carbogen,
375 maintained at 27 °C and superfused (3.5 – 4.5 ml per min) with aCSFcomposed with (mM):
376 129.0 NaCl, 3.35 KCl, 21 $NaHCO_3$, 1.26 $CaCl_2$, 1.15 $MgCl_2$, 0.58 NaH_2PO_4, and 30.0 D-

glucose ("Normal aCSF": pH 7.4) or using the same components except with 10 mM $NaHCO_3$ ("Acidified aCSF": pH 7.1).Inspiratory discharges of respiratory motoneurons were monitored by extracellular recording with glass suction electrodes applied to the proximal cut end of C4 and C3 spinal nerves roots . Axoscope software and Digidata 1320A interface (Axon Instruments, Foster, CA, USA) were used to collect electrophysiological data. Offline analysis was performed with Spike 2 (Cambridge Electronic Design, UK) and Origin 6.0 (Microcal Software, Northampton, MA, USA) software for PC. Burst frequency was analyzed and calculated as the number of C4 bursts per minute. The values of inspiratory burst frequency were calculated as the mean of the last 3 minutes of any condition: ACSF (7.4) and ACSF (7.1). Standardized experiments in WT and *Ndn*-KO preparations were repeated on different preparations from different litters. For a given preparation, only one drug was applied and only one trial was performed.

RT-qPCR

For RT-qPCR, mice were sacrificed at P1, the brainstem dissected, and tissues were rapidly collected and frozen in liquid nitrogen prior to RNA isolation using standard conditions. RNA, reverse transcription and real time PCR were conducted as previously described (Rieusset et al., 2013). Sequences of the various primer pairs used for qPCR, as well as the slope of the calibration curve established from 10 to 1×10^9 copies and qPCR efficiency E, were as follow: *Tph2*: F: 5'-GAGCTTGATGCCGACCAT-3'; R: 5'-TGGCCACATCCACAAAATAC-3'; *Slc6a4*: F:5'-CATATGCTACCAGAATGGTGG-3'; R:5'-AAGATGGCCATGATGGTGTAA-3'. For each sample, the number of cDNA copies was normalized according to relative efficiency of RT determined by the standard cDNA quantification. Finally, gene expression was expressed as the cDNA copy number quantified in 5 µL aliquots of RT product.

Western blot

Newborn mice were sacrificed and brainstems were immediately dissected and snap-frozen in liquid nitrogen and stored at -80 °C until protein extraction. Protein extraction was conducted as previously described (Felix et al. 2012). Membranes were blocked with PBS containing 5 % BSA for 1 h, followed by an overnight incubation at 4 °C with the following primary antibodies: guinea pig anti-SERT (1/2000, Frontier Institute), mouse anti-B3 tubulin (1/2000, ThermoFisher Scientific). Membranes were then washed and incubated 2 h with either anti-guinea pig (1/1000, ThermoFisher Scientific), or anti-mouse (1/2000; DAKO) horseradish peroxidase-conjugated secondary antibodies. Visualisation was performed using the Super signal West-pico chemolumniscent substrate (Pierce, Thermo Scientific, France). Quantification was performed using ImageJ.

Biochemical analysis of the medullary serotonergic system

Pregnant mice were killed by cervical dislocation at gestational day E18.5 and fetuses were removed, decapitated, and the medulla dissected and stored at -80 °C until measurements. Medullary 5-HT, its precursor L-tryptophan (L-Trp), and its main metabolite, 5-hydroxy-indol acid acetic (5-HIAA), were measured with high-pressure liquid chromatography separation and electrochemical detection (Waters System: pump P510, electrochemical detector EC2465; Atlantis column DC18; mobile phase: citric acid, 50 mM; orthophosphoric acid, 50 mM; sodium octane sulfonic acid, 0.112 mM; EDTA, 0.06 mM; methanol, 5%; NaCl, 2 mM; pH 2.95). Contents are expressed in nanograms per medulla.

Raphe primary neuronal culture and live cell uptake assay

Raphe primary cell culture

Newborn mice (n = 6 per culture) were decapitated, brainstems extracted, the meninges removed and the medial part of the brainstem dissected. Tissues were enzymatically digested at 37 °C for 30 minutes with HBSS containing 2 mg/mL of filter-sterilized papain. Cells were resuspended in Neurobasal medium (Thermofisher) containing 2% B27 (Thermofisher), 0.5

427 mM L-glutamine, glucose (50 mM), 50 ng/ml NGF, 10 ng/ml bFGF, 10 µg/ml insulin. 2 x 10^5
428 cells were plated on round 14 mm glass coverslip pre-coated with Polyethyleneimine (20
429 µg/ml). Cells were cultured during 8 days in presence of 5% of NU serum^{TM} (Becton
430 Dickinson) during the first 2 days. Immunocytochemistry was performed to verify presence of
431 5-HT^+ neurons in the culture.

432 *Live cell imaging of* (4-(4-(dimethylamino)styryl)-N-methylpyridinium (ASP+) *uptake*

433 Cells were placed in a bath chamber on the stage of an inverted microscope (Nikon eclipse
434 TE300) and perfused (2 ml/min) with Krebs medium (mM): 150 NaCl; 2.5 KCl; 2 $CaCl_2$; 2
435 $MgCl_2$; 2.5 Hepes acide; 2.5 Hepes-Na; pH 7,4. Time-lapse cell acquisition was started when
436 ASP+ (1, 2, 5, 10, 15 or 20 µM) was added to the perfusion. ASP+ was excited at 488 nm and
437 fluorescence was captured at 607 nm every 10 s for 5 min using Metamorph® software
438 (MolecularDevices). Each ASP+ concentration was tested on 3 different cultures for WT and
439 *Ndn*-KO and 1 for *Ndn*/ *Slc6a4*-DKO. Cells placed on the coverslip were replaced for each
440 concentration tested. For each ASP+ cells, an ROI of the same surface was delineated on the
441 soma in order to measure pixel intensity in arbitrary fluorescence units. 6 ROI were
442 determined at each measurement. Data were background subtracted and ASP+ fluorescence
443 intensity was expressed as a function of initial fluorescence intensity.

444 ***In vivo* recordings of breathing parameters by plethysmography**

445 Breathing of unrestrained, non-anesthetized mice was recorded using constant air flow whole-
446 body plethysmography filled with air or 4% CO_2 in air (EMKA Technologies, Paris, France).
447 Neonatal mice (P0-P1) were recorded in 25 ml chambers (calibrated by injecting 50 µl of air)
448 maintained at neonatal thermoneutral ambient temperature (32 ± 0.5 °C). For adolescent and
449 adult mice (P15-P30-P60), four plethysmography 200ml chambers containing air or
450 (calibrated by injecting 1 ml of air) maintained at 25 ± 0.5 °C were used to allow
451 simultaneous measurements. Analog signals were obtained using an usbAMP device equipped

with 4 inputs and processed using EMKA technologies IOX® software (EMKA Technologies, Paris, France). For neonatal mice, we measured mean respiratory frequency (Rf, expressed in cycles per minute) during quiet periods when mice breathed air or 5 min after breathing hypercapnic air. For adolescent and adult mice respiratory parameters (frequency, tidal volume, minute ventilation) were recorded over 30 minutes after an initial 30 min period of stabilization in the apparatus.,Apnea was defined as a prolonged expiratory time (four times eupneic *expiratory time*), which corresponds to a threshold of 1 sec.

Statistical Analysis

Analyses were performed using two-tailed non-parametric statistical tools due to the size of the samples (GraphPad, Prism software). Values are indicated as following: (Q2 (Q1, Q3), n; statistical test, p-value) where Q2 is the median, Q1 is the first quartile and Q3 is the third quartile and scatter dot plots report Q2 (Q1, Q3). Histograms report the mean±SEM. The level of significance was set at a p-value less than 0.05. Appropriate tests were conducted depending on the experiment and are indicated in the figure legends. Mann-Whitney (MW) test was performed to compare two unmatched groups: differences between WT and *Ndn*-KO (Figure 1 and Figure 2-figure supplement 1). Kolmogorov-Smirnov test was performed to compare the cumulative distribution of two unmatched groups: differences between WT and *Ndn*-KO in apnea accumulation over time (Figure 3E; Figure 3-figure supplement 1E; Figure 3-figure supplement 2E). Chi-square test was performed to compare two groups of animal (WT and *Ndn*-KO) with categorical outcome variable (apnea or no apnea) (Figure 3C; Figure 3-figure supplement 3C). Kruskal-Wallis (KW) followed by a post hoc test Dunn test was performed to compare three or more independent groups (Figure 2G,H; Figure 3D,F-H; Figure 3-figure supplement 1F,H); Friedman test followed by a post hoc test Dunn test was performed to compare matched groups (Figure4-figure supplement 2 C,D). Two-way ANOVA followed by Bonferroni post-hoc test was performed to compare two factors (Figure

2B). Two-way repeated-measure (RM) ANOVA was performed to compare two factors (genotype compared either to time, drug treatment or respiratory challenge) with repeated measure matched by time or respiratory challenge (Figure 3-figure supplement 1D; Figure 3-figure supplement 2D;Figure 4D-F, L and Figure 4-figure supplement 1D); genotype and respiratory challenge. ANCOVA was performed to compare slopes of two regression lines (WT *versus Ndn*-KO: Figure 2E). *: $p< 0.05$; **: $p <0.01$; ***: $p<0.001$; ****: $p<0.0001$.

FIGURE LEGENDS

Figure 1: **Necdin expression in 5-HT neurons and alterations of 5-HT neuronal development and activity in *Ndn*-KO mice**

(**A**) Scheme adapted from (Hawthorne et al., 2010) representing expression profiles of Necdin (green), Pet1 (blue) and 5-HT (red) throughout embryonic development of 5-HT neurons as soon as the progenitors become post-mitotic and start their radial migration by successive waves between E11.5 and E13.5

(**B-C**) 5-HT immunolabelling of brainstem sagittal sections of WT and *Ndn*-KO at E16.5. (**B**) 5-HT nuclei: B4 to B9 (left panels) or B1-B2 (right panels) are abnormal in *Ndn*-KO compared to WT. (**C**) Quantification of 5-HT neurons in the B1-B2 raphe nuclei (WT: 1836 (1751, 1878), n = 8; *Ndn*-KO: 1312 (1234, 1384), n = 7; MW, p = 0.0003).

(**D-E**) **(D)** Brainstem coronal sections of *Pet-EYFP* neurons from E11.5 WT and *Ndn*-KO mice illustrating radial migration from the ventricular zone (V) to the pial surface. (**E**) Quantification of nonlinear migration by measuring the α angle (10 cells/mouse) between the ventricular process and a virtual axis crossing the two opposing points from which neurites extend from the soma: (Angle (°): WT: 1.1 (0.5, 3.5), n = 4; *Ndn*-KO: 18 (2.8, 93.5), n = 3; MW, $p<0.0001$).

(**F-H**) Confocal time-lapse analyses of cell migration of *Pet-EYFP* and *Pet-EYFP*/*Ndn*-KO neurons. **(F)** Plots representing the coordinates of individual cell bodies over time illustrate different cell migration patterns in WT (n = 4) and *Ndn*-KO (n = 3) *Pet-EYFP* neurons (11 cells/mouse). (**G**) Tortuosity index was increased by 52% in *Ndn*-KO compared to WT mice (WT: 1.08 (1.01, 1.26); *Ndn*-KO: 1.65 (1.36, 1.93); MW, p=0.0005). (**H**) Velocity was decreased by 37% in *Ndn*-KO compared to WT (Velocity ($\mu m.s^{-1}$): WT: 2.50 10^{-3} (2.00, 2.93); *Ndn*-KO: 1.57 10^{-3} (1.09, 2.00); MW, p<0.0001).

(**I-K**) Current clamp recordings of *Pet-EYFP* neurons (2 cells/slice) in WT (n = 3) and *Ndn*-KO (n = 3) brain slices. (**I**) Spontaneous discharge pattern of *Pet-EYFP* neurons; (**J-K**) Firing rate **(J)** and resting membrane potential **(K)** in *Ndn*-KO cells and aged-matched WT controls. Frequency (Hz): WT: 2.50 (1.20, 2.50); *Ndn*-KO (4.60 (4.00, 7.90); MW, p = 0.0025; Voltage (mV): WT: -44.37 (-46.25, -43.76); *Ndn*-KO: -42.64 (-43.03, -42.55); MW test, p = 0.0002. Scatter dot plots, report Q2 (Q1, Q3). **: P<0.01; ***: P<0.001.

Figure 1-figure supplement 1: Necdin expression compared with Pet-1 and 5-HT expression throughout embryonic development and alteration of 5-HT projections in *Ndn*-KO embryos.

(**A-I**) Co-expression in WT brainstem of Necdin **(B, E, H)** with Pet-1 **(A)** and 5-HT **(D,G)** at E10.5 **(A-C)**, E12.5 **(D-F)** and E16.5 **(G-I)**.

(**J**) 5-HT IHC on coronal brainstem sections at E12.5 showing 5-HT somas close to the ventricle (right panels) and their axonal projections in the mesencephalon (left panels). Increased somatic labeling concomitant with reduced labeling of the projections is observed in *Ndn*-KO embryos compared with WT.

Figure 1-video 1: Two-photon timelapse video showing somal translocation on organotypic slice cultures of Pet-EYFP neurons in WT embryos (E12.5).

Figure 1-video 2: Two-photon timelapse video showing somal translocation on organotypic slice cultures of Pet-EYFP neurons in *Ndn*-KO embryos (E12.5).

Figure 2: Large punctiform axonal 5-HT staining (5-HT LPAs) results from an increase in SERT expression and activity in *Ndn*-KO mice

(**A-B**) (A) Axonal 5-HT immunoreactivity illustrating 5-HT LPAs in the raphe of WT, *Ndn*-KO, *Slc6a4*-KO and *Ndn*/*Slc6a4*-DKO neonates (P1). (**B**) 5-HT LPAs were counted for all different genotypes (n=3/genotype) in the raphe nuclei (B1-B2, B3, B7, B9), cortex and hippocampus. : Raphe B1-B2: WT: 2.2±0.4; *Ndn*-KO: 11.8±0.8, p=0.003; Raphe B3: WT: 2.6±0.8; *Ndn*-KO: 9.3±1.6, p=0.01; Raphe B7: WT: 6.5±1.2; *Ndn*-KO: 15.5±2.6, p=0.07; Raphe B9: WT: 5.1±2.72; *Ndn*-KO: 14.6±2.9, p=0.0001; Cortex: WT: 5.9±2.0; *Ndn*-KO: 13.4±0.8, p=0.01; Hippocampus: WT: 4.5±1.2; *Ndn*-KO: 11.8±2.5, p=0.01. p-values determined by two-way ANOVA followed by Bonferroni post-hoc test. DKO : double KO. Bar graphs represent mean±SEM.

(**C-D**) (**C**)Western blot analysis of SERT protein expression in brainstem collected from WT, *Ndn*-KO and *Slc6a4*-KO (negative control) neonates (P1). (**D**) Quantification of SERT expression normalized to β3 tubulin expression: WT: 0.45(0.29, 0.56), n=5; *Ndn*- KO: 1.11(0.75, 1.68), n=4; MW, p=0.016). Scatter dot plots, report Q2 (Q1, Q3).

(**E-H**) Real time and single living cell analyses of SERT uptake activity using the fluorescent substrate ASP+, a fluorescent substrate of SERT. **(E)** Kinetic experiment recordings of accumulation of ASP+ over time (5 minutes recording). Coefficient of Determination R^2: WT=0.97; *Ndn* KO= 0.99; *Slc6a4*-KO= 0.93. Mean velocity (v) of ASP+ accumulation obtained by linear regression analyses of the slopes: ($AUF.s^{-1}$): WT: 0.36 ± 0.01, n=18; *Ndn*-

KO: 0.51± 0.01, n=18, covariance (ANCOVA), p<0.0001. Non-specific accumulation of ASP+ fluorescence was evaluated in *Slc6a4*-KO neurons and found to be strongly low (0.02± 0.01 (n=6 cells). (**F**) Saturation experiments using gradual concentration of APS+. Non-linear curve-fitting yielded a one-phase exponential association, with a Vmax (**G**) and Km (**H**) : Vmax (AUF.s^{-1}): WT: 0.45 ± 0.05, n=64; *Ndn*-KO: 0.84± 0.12, n=67; *Slc6a4*-KO: 0.01± 0.03, n=37, p<0.0001; Km (μM): WT: 6.03 ±1.60, n=64; *Ndn*-KO: 12.03± 3.55, n=67; *Slc6a4*-KO: 1.83± 1.60, n=37, p<0.0001. AUF: arbitrary unit of fluorescence. p-values determined by K-W test, followed by Dunn post-hoc test. Bar graphs represent mean±SEM. *: p < 0.05; **: p <0.01; ***: p<0.001.

Figure 2-figure supplement 1: 5-HT metabolism, *Tph2* and *Slc6a4* transcripts quantification in *Ndn*-KO mice.

(**A-D**) 5-HT metabolic analyses from medulla extracted from WT (n=8) and *Ndn*-KO (n=6) mice (at E18.5): **(A)** 5-HT substrate (L-Trp) (mg per gram of tissue): WT: 85.8 (64.5, 98.5); *Ndn*-KO: 83.6 (80.7, 11.2);MW, p= 0.83, N.S. **(B)** 5-HT (ng per gram of tissue): WT: 877.5 (587.4, 1099); *Ndn*-KO: 826.5 (596.1, 1399.0); MW, p> 0.99, N.S.). **(C)** The first metabolite of 5-HT (5-hydroxyindoacetic acid, 5-HIAA) (ng per gram of tissue): WT: 672.8(541.1, 733.4); *Ndn*-KO: 1444 (1354, 1579); MW, p=0.0007. The significant increase of 5-HIAA in *Ndn*-KO conducts to a high 5HIAA/5-HT ratio: WT: 0.8 (0.6, 1.0); *Ndn*-KO: 1.8 (1.1, 2.3); MW, p=0.02.

(**E-F**) RT-qPCR analyses of *Tph2* and *Slc6a4* transcripts in *Ndn*-KO (n=14) and WT (n=13) brainstems of neonate mice (P1). (E) *Tph2* cDNA copies: WT: 9259 (7864, 14567); *Ndn*-KO: 8295 (7955, 9141), MW, p= 0.12, N.S. (F) *Slc6a4* cDNA copies: WT: 5541 (4974, 6720); *Ndn*-KO: 4149 (3228, 6629), MW, p= 0.15, N.S. Neither *Tph2* nor *Slc6a4* presented differences between WT and *Ndn*-KO mice.

Scatter dots represent Q2 (Q1, Q3). N.S.: non-significant; *: $p < 0.05$; ***: $p<0.001$.

Figure 2-figure supplement 2: ASP+ uptake in neurons of raphe primary cultures

(**A**) 5-HT immunocytochemistry on primary raphe cultures showing positive 5-HT neurons (red).

(**B**) Time lapse illustration of ASP+ fluorescence (black) accumulation into cells bodies and fibers over 5 min of recording (t=0; 2; 5 min).

Figure 2-figure supplement 3: Flow diagram of mice used for *in vitro* and *in situ* analyses in figure 1 and 2 and their corresponding supplement figures.

Figure 3: Genetic ablation or pharmacologic inhibition of SERT suppresses apnea and rescues central chemoreflex in *Ndn*-KO mice.

(A) Workflow experiment of constant airflow whole body plethysmography performed in unanaesthetized, unrestrained WT, *Ndn-KO*, *Ndn*/*Slc6a4*-DKO and *Ndn-KO+Fluox* mice at the age of P15. *Ndn*-KO and WT animals (indicated here and in the figure as WT or *Ndn*-KO) have been pre-treated with 0.9% NaCl from age P5 to P15. *Ndn-KO* mice (indicated here and in the figure as *Ndn*-KO+Fluox) have been pre-treated with with Fluoxetine (10mg/Kg/day) from age P5 to P15.

(B) Plethysmographic recordings of WT, *Ndn*-KO, *Ndn*/*Slc6a4*-DKO and *Ndn*-KO+Fluox mice at the age of P15.

(C-E) Quantification of apnea in P15 mice. **(C)** Proportion of apneic mice : WT: 2 of 8; *Ndn*-KO: 7 of 8; corresponding respectively to 25% and 87%; Chi^2 test, p=0.01. Genetic ablation of *Slc6a4*or early Fluoxetine treatment normalized the number of *Ndn-KO* apneic mice: *Ndn*/*Slc6a4* DKO: 2 of 8, 25%; Chi^2 test, p>0.99, N.S.; *Ndn*-KO+Fluox: 2 of 8, 25%; Chi^2 test,

p>0.99, N.S. **(D)** Number of apnea in *Ndn-KO* compared to WT mice: WT: 0.0 (0.0, 1.5), n=8; *Ndn*-KO: 3.8 (2.0, 8.0), n=8; p=0.01. Genetic ablation of *Slc6a4* or Fluoxetine treatment normalized the number of apnea of *Ndn*-KO mice to WT values: *Ndn*/*Slc6a4*-DKO: 0.0 (0.0, 2.0), n=8; p>0.99, N.S.; *Ndn*-KO+Fluox: 0.0 (0.0, 2.2), n=8; p>0.99, N.S. p-values determined by KW test followed by Dunn post-hoc test with comparison to WT. **(E)** Cumulative distribution of apnea (number of cumulated values) over apnea duration (msec) in WT, *Ndn*-KO, *Ndn*/ *Slc6a4*-DKO and *Ndn*-KO treated by Fluoxetine. Compared to WT, *Ndn*-KO mice demonstrated a significant increase of cumulative apnea both in term of number and duration (Kolmogorov-Smirnov test, p=0.01). However, such increase was normalized to WT after genetic deletion of *Slc6a4* or Fluoxetine treatment.

(**F-H**) Basic breathing parameters: **(F)** Minute ventilation, VE (the total volume breathed over one min): WT: 24.5 (17.7, 32.7), n=8; *Ndn*-KO: 17.5 (15.2, 18.7), n=8; p=0.14, N.S.; *Ndn*/ *Slc6a4*-DKO: 18.0 (17.0, 20.0), n=8; p=0.25, N.S. and *Ndn*-KO+Fluox: 21.0 (18.2, 29.7), n=8; p>0.99, N.S.. **(G)** Frequency of breathing, Rf (breaths/min): WT: 338 (312, 3867), n=8; *Ndn*-KO: 296 (270, 352), n=8; p=0.56, N.S.; *Ndn*/ *Slc6a4*-DKO: 292 (2890, 305), n=8; p=0.16, N.S. and *Ndn*-KO+Fluox: 329 (289, 388), n=8; p>0.99, N.S. **(H)** Tidal Volume, VT (the volume flow per breath): WT: 0.07 (0.05, 0.09), n=8; *Ndn*-KO: 0.06 (0.06, 0.06), n=8; p=0.38, N.S.; *Ndn*/ *Slc6a4*-DKO: 0.06 (0.05, 0.07), n=8; p=0.51, N.S. and *Ndn*-KO+Fluox: 0.07 (0.06, 0.08), n=8; p>0.99, N.S.

p-values determined by K-W test followed by Dunn post-hoc test with comparison to WT.Scatter dots represent Q2 (Q1, Q3). N.S.: non-significant; *: $p < 0.05$.

Figure 3-figure supplement 1: Early life Fluoxetine treatment has only short-term positive effects on *Ndn*-KO apneas.

(A) Workflow experiment of constant airflow whole body plethysmography performed in unanaesthetized, unrestrained WT and *Ndn-KO* mice at 0, 15 and 45 days after treatment (DAT). *Ndn*-KO and WT animals (indicated here and in the figure as WT or *Ndn*-KO) have been pre-treated with 0.9% NaCl from age P5 to P15. *Ndn-KO* mice (indicated here and in the figure as *Ndn*-KO+Fluox) have been pre-treated with Fluoxetine (10mg/Kg/day) from age P5 to P15.

(B) Plethysmographic recordings of early Fluoxetine treated *Ndn*-KO mice at 45 DAT showing apnea.

(C) In the WT and *Ndn*-KO groups, the prevalence of mice with apnea did not change over time, although a significantly proportion of apneic mice were found in *Ndn*-KO group compared to WT group. Comparison of the proportion of apneic mice over post-treatment time points between *Ndn*-KO treated groups (vehicle or Fluoxetine) confirmed that at 0 DAT, Fluoxetine significantly decreased the prevalence of *Ndn-KO* apneic mice (*Ndn-KO*+vehicle: 0 of 6, 100%; *Ndn-KO*+Fluox: 1 of 6; 16%, n= 6; Chi^2, p=0.01), to similar level of WT (WT: 1 of 6; 16%). However, this difference was not anymore observed at 15 DAT (*Ndn-KO*+vehicle: 1 of 6; 16 %; *Ndn-KO*+Fluox: 2 of 6; 33%, n= 6; Chi^2, p=0.66, N.S.) and 45 DAT *(Ndn-KO*+vehicle: 1 of 6; 16%; *Ndn-KO*+Fluox: 1 of 6; 16%, n= 6; Chi^2, p=1.0, N.S.). N.S.: non-significant; **: $p < 0.01$.

(D) Number of apnea over time (0, 15, 45 DAT) in the different mice groups. Except for WT group which values were stable over time, vehicle or Fluoxetine-treated *Ndn*-KO mice present an increase in the number of apnea over time which appears significant at 45 DAT compared to 0 DAT: *Ndn*-KO (0 DAT: 7(1.5, 10); 45 DAT: 27(18, 31); n=6, p=0.001); *Ndn*-KO+Fluox (0 DAT: 0(0, 0.75); 45 DAT: 21(6, 32); n=6, p=0.001). Comparison between the *Ndn*-KO treated groups (vehicle or Fluoxetine) confirmed significant difference in the number of apnea at 0 DAT (p=0.041) but revealed non-significant difference at 15 DAT (*Ndn*-KO: 3(0, 10);

650 *Ndn*-KO+Fluox: 5(0, 9), p>0.99; N.S.) and 45 DAT (*Ndn*-KO: 27(18, 31); *Ndn*-KO+Fluox:
651 21(6, 32), p= 0.75; N.S.). P-values determined by two-way repeated-measure (RM) ANOVA
652 followed by Bonferroni post-hoc test. Scatter dots represent Q2 (Q1, Q3). N.S.: non-
653 significant; *: $p < 0.05$.
654 **(E)** Cumulative distribution of apnea (number of cumulated values) over apnea duration
655 measured in WT, *Ndn*-KO and *Ndn*-KO treated with Fluoxetine (45 DAT). At this stage, the
656 distribution of apnea duration appeared similar between treated and untreated *Ndn*-KO mice
657 suggesting that early life Fluoxetine treatment in *Ndn*-KO had no long term effect on apnea in
658 those animals. Both *Ndn*-KO groups (vehicle or Fluoxetine-treated) appeared significantly
659 different to WT (p=0.0001, Kolmogorov-Smirnov test). ****: p<0.0001
660 (**F-H**) Breathing parameters measured at 45 DAT: **(F)** Minute ventilation, VE: WT: 76.5
661 (61.5, 88.7), n=8; *Ndn*-KO: 58.5 (41.7, 64.2), n=6; p=0.16, N.S.; and *Ndn*-KO+Fluox: 65.0
662 (48.7, 105.3), n=6; p=0.96, N.S.; **(G)** Frequency of breathing, Rf: WT: 469 (4067, 531), n=8;
663 *Ndn*-KO: 368 (302, 460), n=6; p=0.13, N.S.; and *Ndn*-KO+Fluox: 450 (402, 579), n=6;
664 p>0.99, N.S; **(H)** Tidal Volume, VT: WT: 0.17 (0.15, 0.18), n=8; *Ndn*-KO: 0.14 (0.13, 0.16),
665 n=6; p=0.25, N.S.; and *Ndn*-KO+Fluox: 0.16 (0.11, 0.18), n=6; p=0.89, N.S p-values
666 determined by K-W test followed by Dunn post-hoc test with comparison to WT. Scatter dots
667 represent Q2 (Q1, Q3).
668
669 **Figure 3-figure supplement 2: Early life treatment of Fluoxetine on respiratory apnea in**
670 **wild-type mice.**
671 **(A-B)** Plethysmographic recordings of WT mice at 45DAT pre-treated either with **(A)** 0.9%
672 NaCl (indicated here as WT) or **(B)** Fluoxetine (indicated here as WT+Fluox) (10mg/Kg/day)
673 from age P5 to P15 (see workflow in Figure 3-supplement 1). Note in B the appearance of
674 apnea for WT mice, which received the treatment. **(C)** Proportion of apneic mice, at 0, 15 and

45 DAT, in Fluoxetine-treated WT mice compared with WT mice: 0 DAT: WT= 1 of 8, 12.5%, WT+Fluox: 6 of 8, 75%; Chi^2 , p=0.011; 15 DAT: WT= 1 of 8, 12.5%, WT+Fluox: 6 of 8, 75%; Chi^2 , p= 0.011; 45 DAT: WT= 3 of 8, 37.5% WT+Fluox: 8 of 8, 100%; Chi^2 , p= 0.010. (**D**) Number of apnea per hour at different DAT: 0; 15; 45 in Fluoxetine-treated and WT groups. Except for WT group whose values were stable over time, we found for Fluoxetine-treated WT mice a significant increase of the number of apnea over time (0 DAT: 2(0.5, 2); 15 DAT: 2(0.5, 5.5); 45 DAT: 12(8.5, 24.5); p<0.0001). Comparison between both WT groups confirmed significant difference in the number of apnea at 15 DAT (WT: 0 (0.2); WT+fluox: 12(8.5, 24.5)) p<0.0001). p-values determined by two-way RM ANOVA followed by Bonferroni post-hoc test.

(**E**) Cumulative distribution of apnea (number of cumulated values) over apnea duration measured at 45 DAT in WT and WT treated with Fluoxetine. Fluoxetine treatment produces a significant increase in apnea accumulation over apnea duration (Kolmogorov-Smirnov test, p=0.0001).

*: p <0.05; **: p <0.01; ****: p<0.0001.

Figure 4: Alteration of respiratory chemoreflex in *Ndn*-KO neonates is rescued by Fluoxetine.

(A-F) Effect of hypercapnia on *in vivo* ventilatory parameters of WT and *Ndn*-KO neonates.

(**A**) Workflow experiment of constant airflow whole body plethysmography performed in unanaesthetized, unrestrained WT, *Ndn-KO* neonates at P0-P1 when breathing either air or hypercapnic mixture containing 4% CO2 in air for 5 min. Data for analyses were collected in the last 5 min (air) or the last min (hypercapnia).

699 (**B-C**) **(B)** Plethysmographic recordings of WT and *Ndn*-KO neonates when breathing air or
700 **(C)** at 5th min upon hypercapnic respiratory challenge.
701 **(D)** Respiratory frequency (Rf) in WT and *Ndn*-KO pups when subjected to hypercapnic
702 stress: WT Air: 91 ±8; WT hypercapnia: 163± 16; n=8, p=0.004; *Ndn*-KO Air: 95 ±12; *Ndn*-
703 KO hypercapnia: 123± 11; n=8, p=0.31, N.S. p-values determined by two-way-ANOVA test
704 followed by Bonferroni post-hoc test. Bar graphs represent mean±SEM; **: p<0.01; N.S.:
705 non-significant.
706 (**E**) Tidal Volume (VT) ($\mu l.g^{-1}$) in WT neonates: WT Air: 9 ±0.7; WT hypercapnia: 12±1;
707 n=8, p=0.12 N.S.; in *Ndn*-KO: *Ndn*-KO Air: 7.5±0.9; *Ndn*-KO hypercapnia: 10.9±1.1; n=8,
708 p=0.055. p-values determined by two-way ANOVA test followed by Bonferroni post-hoc test.
709 (**F**) Minute Ventilation (VE) ($ml.min^{-1}.g^{-1}$) in WT neonates: WT Air: 0.8±0.1; WT
710 hypercapnia: 2.1±0.1; n=8, p=0.01; in *Ndn*-KO: *Ndn*-KO Air: 0.7±0.1; *Ndn*-KO hypercapnia:
711 1.3±0.2; n=8, p=0.3 N.S. p-values determined by two-way ANOVA test followed by
712 Bonferroni post-hoc test. Bar graphs represent mean±SEM. *: p<0.05.
713 **(G-H)** Effect of Fluoxetine treatment on the resting phrenic burst frequency (PBf) and the
714 PBf response to acidosis in *Ndn*-KO medulla preparations.
715 **(G)** Electrophysiological recordings of PBf produced *in vitro* in WT and *Ndn*-KO *en bloc*
716 brainstem-spinal cord preparations at P0-P1 when superfused first with neutral artificial
717 cerebrospinal fluid (aCSF) (pH 7.4) and then acidified aCSF (pH 7.1)**.** (**H**) Workflow
718 experiment of the electrophysiological recordings on medullary preparations to assess central
719 chemosensitivity in WT and treated with Fluoxetine (20μM) or untreated *Ndn*-KO mice.
720 (**I-K**) Examples of continuous electrophysiological recordings of rhythmic phrenic bursts
721 produced in *en bloc* brainstem-spinal cord preparations of **(I)** one WT, **(J)** one *Ndn*-KO and
722 **(K)** one *Ndn*-KO treated with Fluoxetine (20 μM) pup and superfused with first neutral aCSF
723 (pH 7.4) (left column recordings) or acidified aCSF (pH 7.1) (right column recordings).

(L) Quantifications of the resting PBf (c.min^{-1}) of *en bloc* preparations superfused with neutral aCSF (pH 7.4) or acidified aCSF (pH 7.1) respectively of WT (WT (pH 7.4): 8.8 c.min^{-1} ± 1.2; WT (pH 7.1) 12.8 ± 0.3 c.min^{-1}; n=12, p<0.001), *Ndn*-KO (*Ndn*-KO (pH 7.4)*:* 9.5 ± 1.0; *Ndn*-KO (pH 7.1): 9.8± 0.3 c.min^{-1}; n=12, p=0.41, N.S.) and *Ndn*-KO treated with Fluoxetine: (*Ndn*-KO+ Fluox (pH 7.4): 9.6± 0.3; *Ndn*-KO+Fluox (pH 7.1): 12.6± 0.7; n=12, p=0.04). Noticeably, under neutral aCSF (pH 7.4) no difference was observed between WT, *Ndn*-KO and *Ndn*-KO+ Fluox. However, in acidified aCSF (pH 7.1), Fluoxetine significantly increased the PBf of *Ndn*-KO preparations. p-values determined by two-way ANOVA test followed by Tukey post-hoc test. Bar graphs represent mean±SEM. N.S: non-significant; *: p < 0.05;

Figure 4 –Source DATA 1: Plethysmography data before and after hypercapnia in WT and *Ndn*-KO mice.

Figure 4 –Source DATA 2: Electrophysiology data of rhythmic phrenic bursts frequency during acidosis in WT and *Ndn*-KO preparations - before and after Fluoxetine treatment.

Figure 4-figure supplement 1: Effect of pre-treatment with the 5-HT1A-R agonist 8OHDPAT on the resting PBf and the PBf response to acidosis in *Ndn*-KO *en bloc* brainstem-spinal cord preparations of P0-P1 pups.

(**A-C**) PBf produced in *Ndn*-KO ***en bloc*** brainstem-spinal cord preparations superfused with **(A)** neutral aCSF (pH 7.4) and then treated with 8OHDPAT (1µM) either **(B)** in neutral aCSF (pH 7.4) or **(C)** in acidified aCSF (pH 7.1).

(**D**) Quantifications of the PBf (c.min^{-1}) of *en bloc* brainstem-spinal cord preparations superfused with neutral aCSF (pH 7.4) and acidified aCSF (pH 7.1) of *Ndn*-KO (*Ndn*-KO (pH 7.4): 10.2±1.5; *Ndn*-KO (pH 7.1): 9.9±0.3; p=0.99, N.S.); and *Ndn*-KO treated with 8OHDPAT (*Ndn*-KO+8OHDPAT (pH 7.4): 13.2±1.9; *Ndn*-KO+8OHDPAT (pH 7.1):

16.5±2.6, n=13; p=0.04). In neutral aCSF (pH 7.4), 8OHDPAT did not affect PBf in *Ndn*-KO preparation. However, similarly to Fluoxetine, in acidified aCSF (pH 7.1), 8OHDPAT significantly increased the PBf of *Ndn*-KO preparations. p-values determined by two-way ANOVA test followed by Tukey post-hoc test.

Bar graphs represent mean±SEM. N.S.: non-significant; *: $p < 0.05$

Figure 4-figure supplement 2: Effects of Fluoxetine and of the 5-HT1A-R agonist 8OHDPAT on the resting PBf and the PBf response to acidosis in wild-type medulla preparations.

(**A-B**) PBf produced in WT ***en bloc*** brainstem-spinal cord preparations superfused with **(A)** neutral aCSF (pH 7.4) and treated with Fluoxetine (20µM) in aCSF (pH 7.4) or acidified aCSF (pH 7.1), **(B)** neutral aCSF (pH 7.4) and treated with 8OHDPAT (1µM) in aCSF (pH 7.4) or acidified aCSF (pH 7.1). Note the absence of PBf response upon acidosis.

C-D) Quantifications of the PBf ($c.min^{-1}$) of *en bloc* brainstem-spinal cord preparations of WT pups untreated and superfused with neutral aCSF (pH 7.4) or acidified aCSF (pH 7.1) and treated with **(C)** Fluoxetine (20µM): WT (pH 7.4): 8.8±1.2; WT+Fluox (pH 7.4): 8.2±1.0, p>0.99, N.S.; WT+Fluox (pH 7.1): 7.8±0.7; n=12, p>0.99, N.S.) or treated with **(D)** 8OHDPAT (1 µM) WT (pH 7.4): 11.0±1.1; WT+ 8OHDPAT (pH 7.4): 12.3±2.4, p=0.76, N.S.; WT+ 8OHDPAT (pH7.1): 12.7±3.3; n=8, p=0.63, N.S. p-values determined by Friedman test followed by Dunn post-hoc test with comparison to WT. Bar graphs represent mean±SEM. N.S.: non-significant.

Figure 4 –Source DATA 3: Relates to Figure 4-figure supplements 1 and 2. Electrophysiology data of rhythmic phrenic bursts frequency during acidosis in WT and *Ndn*-KO preparations - before and after 8-OHDPAT treatment.

Figure 4 – figure supplement 3: Flow diagram of mice used for *ex vivo* and *in vivo* analyses in figure 3 and 4 and their corresponding supplement figures.

REFERENCES

Abdala, A.P., Dutschmann, M., Bissonnette, J.M., and Paton, J.F. (2010). Correction of respiratory disorders in a mouse model of Rett syndrome. *Proc Natl Acad Sci U S A* **107**, 18208-18213.

Aebischer, J., Sturny, R., Andrieu, D., Rieusset, A., Schaller, F., Geib, S., Raoul, C., and Muscatelli, F. (2011). Necdin protects embryonic motoneurons from programmed cell death. *PLoS ONE* **6**, e23764.

Andrieu, D., Meziane, H., Marly, F., Angelats, C., Fernandez, P.A., and Muscatelli, F. (2006). Sensory defects in Necdin deficient mice result from a loss of sensory neurons correlated within an increase of developmental programmed cell death. *BMC Dev Biol* **6**, 56.

Andrieu, D., Watrin, F., Niinobe, M., Yoshikawa, K., Muscatelli, F., and Fernandez, P.A. (2003). Expression of the Prader-Willi gene Necdin during mouse nervous system development correlates with neuronal differentiation and p75NTR expression. *Gene Expr Patterns* **3**, 761-765.

Arens, R., Gozal, D., Burrell, B.C., Bailey, S.L., Bautista, D.B., Keens, T.G., and Ward, S.L. (1996). Arousal and cardiorespiratory responses to hypoxia in Prader-Willi syndrome. *Am J Respir Crit Care Med* **153**, 283-287.

Barrett, K.T., Dosumu-Johnson, R.T., Daubenspeck, J.A., Brust, R.D., Kreouzis, V., Kim, J.C., Li, A., Dymecki, S.M., and Nattie, E.E. (2016). Partial Raphe Dysfunction in Neurotransmission Is Sufficient to Increase Mortality after Anoxic Exposures in Mice at a Critical Period in Postnatal Development. *J Neurosci* **36**, 3943-3953.

Berner, J., Shvarev, Y., Zimmer, A., and Wickstrom, R. (2012). Hypoxic ventilatory response in Tac1-/- neonatal mice following exposure to opioids. *J Appl Physiol (1985)* **113**, 1718-1726.

Butler, M.G., Manzardo, A.M., Heinemann, J., Loker, C., and Loker, J. (2017). Causes of death in Prader-Willi syndrome: Prader-Willi Syndrome Association (USA) 40-year mortality survey. *Genet Med* **19**, 635-642.

Cohen, M., Hamilton, J., and Narang, I. (2014). Clinically important age-related differences in sleep related disordered breathing in infants and children with Prader-Willi Syndrome. *PLoS ONE* **9**, e101012.

Duncan, J.R., Paterson, D.S., Hoffman, J.M., Mokler, D.J., Borenstein, N.S., Belliveau, R.A., Krous, H.F., Haas, E.A., Stanley, C., Nattie, E.E*., et al.* (2010). Brainstem serotonergic deficiency in sudden infant death syndrome. *Jama* **303**, 430-437.

Festen, D.A., de Weerd, A.W., van den Bossche, R.A., Joosten, K., Hoeve, H., and Hokken-Koelega, A.C. (2006). Sleep-related breathing disorders in pre-pubertal children with Prader-Willi Syndrome and effects of growth hormone treatment. *J Clin Endocrinol Metab*.

Gerard, M., Hernandez, L., Wevrick, R., and Stewart, C.L. (1999). Disruption of the mouse necdin gene results in early post-natal lethality. *Nat Genet* **23**, 199-202.

Gillett, E.S., and Perez, I.A. (2016). Disorders of Sleep and Ventilatory Control in Prader-Willi Syndrome. *Diseases* **4**.

Glover, M.E., and Clinton, S.M. (2016). Of rodents and humans: A comparative review of the neurobehavioral effects of early life SSRI exposure in preclinical and clinical research. *Int J Dev Neurosci* **51**, 50-72.

Gozal, D., Arens, R., Omlin, K.J., Ward, S.L., and Keens, T.G. (1994). Absent peripheral chemosensitivity in Prader-Willi syndrome. *J Appl Physiol (1985)* **77**, 2231-2236.

Hawthorne, A.L., Wylie, C.J., Landmesser, L.T., Deneris, E.S., and Silver, J. (2010). Serotonergic neurons migrate radially through the neuroepithelium by dynamin-mediated somal translocation. *J Neurosci* **30**, 420-430.

Hilaire, G., Voituron, N., Menuet, C., Ichiyama, R.M., Subramanian, H.H., and Dutschmann, M. (2010). The role of serotonin in respiratory function and dysfunction. *Respir Physiol Neurobiol* **174**, 76-88.

Hodges, M.R., and Richerson, G.B. (2008). Contributions of 5-HT neurons to respiratory control: neuromodulatory and trophic effects. *Respir Physiol Neurobiol* **164**, 222-232.

Holtman, J.R., Jr., and Speck, D.F. (1994). Substance P immunoreactive projections to the ventral respiratory group in the rat. *Peptides* **15**, 803-808.

Kachidian, P., Poulat, P., Marlier, L., and Privat, A. (1991). Immunohistochemical evidence for the coexistence of substance P, thyrotropin-releasing hormone, GABA, methionine-enkephalin, and leucin-enkephalin in the serotonergic neurons of the caudal raphe nuclei: a dual labeling in the rat. *J Neurosci Res* **30**, 521-530.

Kinney, H.C., Broadbelt, K.G., Haynes, R.L., Rognum, I.J., and Paterson, D.S. (2011). The serotonergic anatomy of the developing human medulla oblongata: implications for pediatric disorders of homeostasis. *J Chem Neuroanat* **41**, 182-199.

Kuwajima, T., Hasegawa, K., and Yoshikawa, K. (2010). Necdin promotes tangential migration of neocortical interneurons from Basal forebrain. *J Neurosci* **30**, 3709-3714.

Kuwako, K., Hosokawa, A., Nishimura, I., Uetsuki, T., Yamada, M., Nada, S., Okada, M., and Yoshikawa, K. (2005). Disruption of the paternal necdin gene diminishes TrkA signaling for sensory neuron survival. *J Neurosci* **25**, 7090-7099.

Lau, T., Proissl, V., Ziegler, J., and Schloss, P. (2015). Visualization of neurotransmitter uptake and release in serotonergic neurons. *J Neurosci Methods* **241**, 10-17.

Lee, S., Walker, C.L., Karten, B., Kuny, S.L., Tennese, A.A., O'Neill, M.A., and Wevrick, R. (2005). Essential role for the Prader-Willi syndrome protein necdin in axonal outgrowth. *Hum Mol Genet* **14**, 627-637.

Liu, X., Wang, Y., Zhang, Y., Zhu, W., Xu, X., Niinobe, M., Yoshikawa, K., Lu, C., and He, C. (2009). Nogo-A inhibits necdin-accelerated neurite outgrowth by retaining necdin in the cytoplasm. *Mol Cell Neurosci* **41**, 51-61.

Maejima, T., Masseck, O.A., Mark, M.D., and Herlitze, S. (2013). Modulation of firing and synaptic transmission of serotonergic neurons by intrinsic G protein-coupled receptors and ion channels. *Front Integr Neurosci* **7**, 40.

Millard, S.J., Weston-Green, K., and Newell, K.A. (2017). The effects of maternal antidepressant use on offspring behaviour and brain development: implications for risk of neurodevelopmental disorders. *Neurosci Biobehav Rev*.

Miller, J., and Wagner, M. (2013). Prader-Willi syndrome and sleep-disordered breathing. *Pediatr Ann* **42**, 200-204.

Miller, N.L., Wevrick, R., and Mellon, P.L. (2009). Necdin, a Prader-Willi syndrome candidate gene, regulates gonadotropin-releasing hormone neurons during development. *Hum Mol Genet* **18**, 248-260.

Mouri, A., Sasaki, A., Watanabe, K., Sogawa, C., Kitayama, S., Mamiya, T., Miyamoto, Y., Yamada, K., Noda, Y., and Nabeshima, T. (2012). MAGE-D1 regulates expression of depression-like behavior through serotonin transporter ubiquitylation. *J Neurosci* **32**, 4562-4580.

Muscatelli, F., Abrous, D.N., Massacrier, A., Boccaccio, I., Le Moal, M., Cau, P., and Cremer, H. (2000). Disruption of the mouse Necdin gene results in hypothalamic and behavioral alterations reminiscent of the human Prader-Willi syndrome. *Hum Mol Genet* **9**, 3101-3110.

Nixon, G.M., and Brouillette, R.T. (2002). Sleep and breathing in Prader-Willi syndrome. *Pediatr Pulmonol* **34**, 209-217.

Oz, M., Libby, T., Kivell, B., Jaligam, V., Ramamoorthy, S., and Shippenberg, T.S. (2010). Real-time, spatially resolved analysis of serotonin transporter activity and regulation using the fluorescent substrate, ASP+. *J Neurochem* **114**, 1019-1029.

867 Pagliardini, S., Ren, J., Wevrick, R., and Greer, J.J. (2005). Developmental abnormalities of neuronal
868 structure and function in prenatal mice lacking the prader-willi syndrome gene necdin. *Am J Pathol*
869 **167**, 175-191.
870 Pagliardini, S., Rent, J., Wevrick, R., and Greer, J.J. (2008). Neurodevelopmental abnormalities in the
871 brainstem of prenatal mice lacking the Prader-Willi syndrome gene Necdin. *Adv Exp Med Biol* **605**,
872 139-143.
873 Paterson, D.S., Hilaire, G., and Weese-Mayer, D.E. (2009). Medullary serotonin defects and
874 respiratory dysfunction in sudden infant death syndrome. *Respir Physiol Neurobiol* **168**, 133-143.
875 Pavone, M., Caldarelli, V., Khirani, S., Colella, M., Ramirez, A., Aubertin, G., Crino, A., Brioude, F.,
876 Gastaud, F., Beydon, N.*, et al.* (2015). Sleep disordered breathing in patients with Prader-Willi
877 syndrome: A multicenter study. *Pediatr Pulmonol* **50**, 1354-1359.
878 Ptak, K., Yamanishi, T., Aungst, J., Milescu, L.S., Zhang, R., Richerson, G.B., and Smith, J.C. (2009).
879 Raphe neurons stimulate respiratory circuit activity by multiple mechanisms via endogenously
880 released serotonin and substance P. *J Neurosci* **29**, 3720-3737.
881 Ren, J., Lee, S., Pagliardini, S., Gerard, M., Stewart, C.L., Greer, J.J., and Wevrick, R. (2003). Absence of
882 Ndn, encoding the Prader-Willi syndrome-deleted gene necdin, results in congenital deficiency of
883 central respiratory drive in neonatal mice. *J Neurosci* **23**, 1569-1573.
884 Rieusset, A., Schaller, F., Unmehopa, U., Matarazzo, V., Watrin, F., Linke, M., Georges, B., Bischof, J.,
885 Dijkstra, F., Bloemsma, M.*, et al.* (2013). Stochastic loss of silencing of the imprinted Ndn/NDN allele,
886 in a mouse model and humans with prader-willi syndrome, has functional consequences. *PLoS Genet*
887 **9**, e1003752.
888 Rood, B.D., Calizo, L.H., Piel, D., Spangler, Z.P., Campbell, K., and Beck, S.G. (2014). Dorsal raphe
889 serotonin neurons in mice: immature hyperexcitability transitions to adult state during first three
890 postnatal weeks suggesting sensitive period for environmental perturbation. *J Neurosci* **34**, 4809-
891 4821.
892 Schluter, B., Buschatz, D., Trowitzsch, E., Aksu, F., and Andler, W. (1997). Respiratory control in
893 children with Prader-Willi syndrome. *Eur J Pediatr* **156**, 65-68.
894 Scott, M.M., Krueger, K.C., and Deneris, E.S. (2005a). A differentially autoregulated Pet-1 enhancer
895 region is a critical target of the transcriptional cascade that governs serotonin neuron development. *J*
896 *Neurosci* **25**, 2628-2636.
897 Scott, M.M., Wylie, C.J., Lerch, J.K., Murphy, R., Lobur, K., Herlitze, S., Jiang, W., Conlon, R.A.,
898 Strowbridge, B.W., and Deneris, E.S. (2005b). A genetic approach to access serotonin neurons for in
899 vivo and in vitro studies. *Proc Natl Acad Sci U S A* **102**, 16472-16477.
900 Sedky, K., Bennett, D.S., and Pumariega, A. (2014). Prader Willi syndrome and obstructive sleep
901 apnea: co-occurrence in the pediatric population. *J Clin Sleep Med* **10**, 403-409.
902 Takazaki, R., Nishimura, I., and Yoshikawa, K. (2002). Necdin is required for terminal differentiation
903 and survival of primary dorsal root ganglion neurons. *Exp Cell Res* **277**, 220-232.
904 Tan, H.L., and Urquhart, D.S. (2017). Respiratory Complications in Children with Prader Willi
905 Syndrome. *Paediatr Respir Rev* **22**, 52-59.
906 Tennese, A.A., Gee, C.B., and Wevrick, R. (2008). Loss of the Prader-Willi syndrome protein necdin
907 causes defective migration, axonal outgrowth, and survival of embryonic sympathetic neurons. *Dev*
908 *Dyn* **237**, 1935-1943.
909 Teran, F.A., Massey, C.A., and Richerson, G.B. (2014). Serotonin neurons and central respiratory
910 chemoreception: where are we now? *Prog Brain Res* **209**, 207-233.
911 Toward, M.A., Abdala, A.P., Knopp, S.J., Paton, J.F., and Bissonnette, J.M. (2013). Increasing brain
912 serotonin corrects CO2 chemosensitivity in methyl-CpG-binding protein 2 (Mecp2)-deficient mice.
913 *Exp Physiol* **98**, 842-849.
914 Trowbridge, S., Narboux-Neme, N., and Gaspar, P. (2011). Genetic models of serotonin (5-HT)
915 depletion: what do they tell us about the developmental role of 5-HT? *Anat Rec (Hoboken)* **294**,
916 1615-1623.

Urquhart, D.S., Gulliver, T., Williams, G., Harris, M.A., Nyunt, O., and Suresh, S. (2013). Central sleep-disordered breathing and the effects of oxygen therapy in infants with Prader-Willi syndrome. *Arch Dis Child* **98**, 592-595.

Voituron, N., Shvarev, Y., Menuet, C., Bevengut, M., Fasano, C., Vigneault, E., El Mestikawy, S., and Hilaire, G. (2010). Fluoxetine treatment abolishes the in vitro respiratory response to acidosis in neonatal mice. *PLoS ONE* **5**, e13644.

Zanella, S., Watrin, F., Mebarek, S., Marly, F., Roussel, M., Gire, C., Diene, G., Tauber, M., Muscatelli, F., and Hilaire, G. (2008). Necdin plays a role in the serotonergic modulation of the mouse respiratory network: implication for Prader-Willi syndrome. *J Neurosci* **28**, 1745-1755.

Zhuang, X., Masson, J., Gingrich, J.A., Rayport, S., and Hen, R. (2005). Targeted gene expression in dopamine and serotonin neurons of the mouse brain. *J Neurosci Methods* **143**, 27-32.

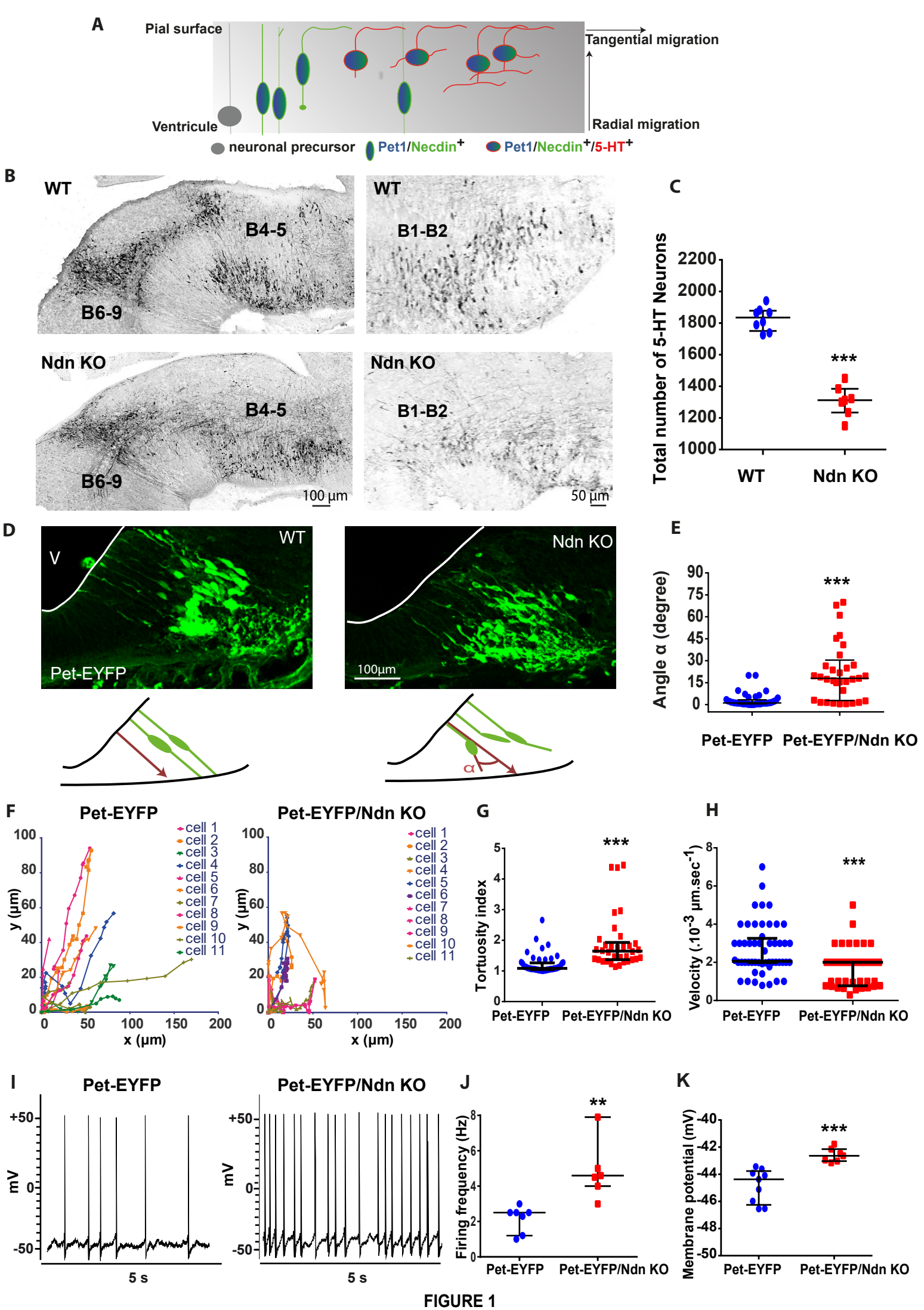
A
Pial surface
Tangential migration
Radial migration
Ventricule
neuronal precursor
Pet1/Necdin+
Pet1/Necdin+/5-HT+
B
WT
B4-5
B6-9
WT
B1-B2
Ndn KO
B4-5
B6-9
100 µm
Ndn KO
B1-B2
50 µm
C
Total number of 5-HT Neurons
2200
2000
1800
1600
1400
1200
1000
***
WT
Ndn KO
D
V
WT
Pet-EYFP
Ndn KO
100µm
α
E
Angle α (degree)
90
75
60
45
30
15
0
***
Pet-EYFP
Pet-EYFP/Ndn KO
F
Pet-EYFP
Pet-EYFP/Ndn KO
y (µm)
x (µm)
cell 1
cell 2
cell 3
cell 4
cell 5
cell 6
cell 7
cell 8
cell 9
cell 10
cell 11
G
Tortuosity index
***
Pet-EYFP
Pet-EYFP/Ndn KO
H
Velocity (.10-3 µm.sec-1)
***
Pet-EYFP
Pet-EYFP/Ndn KO
I
Pet-EYFP
Pet-EYFP/Ndn KO
+50
mV
0
-50
5 s
J
Firing frequency (Hz)
**
Pet-EYFP
Pet-EYFP/Ndn KO
K
Membrane potential (mV)
-40
-42
-44
-46
-48
-50
***
Pet-EYFP
Pet-EYFP/Ndn KO

FIGURE 1

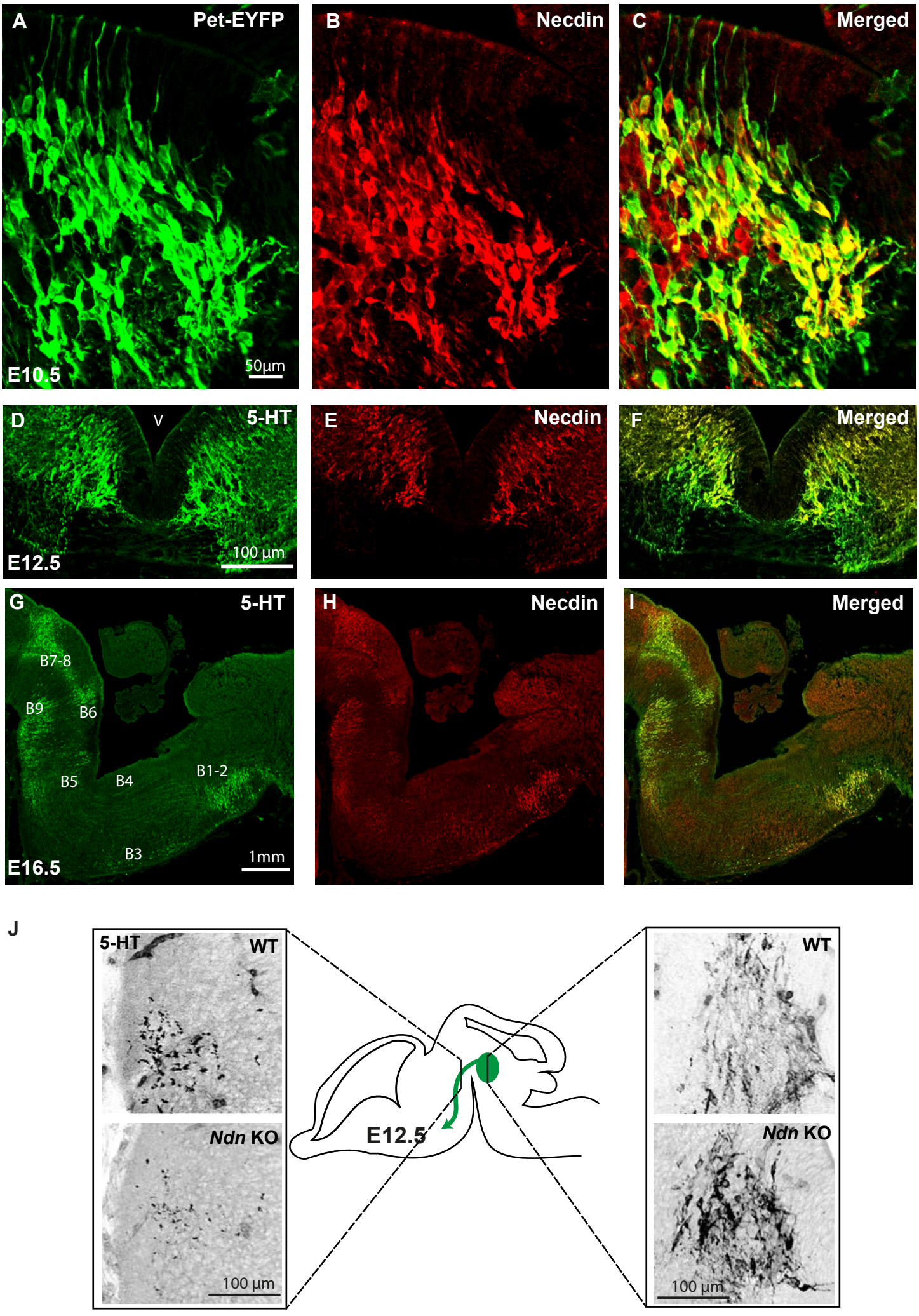

FIGURE 1-Sup 1

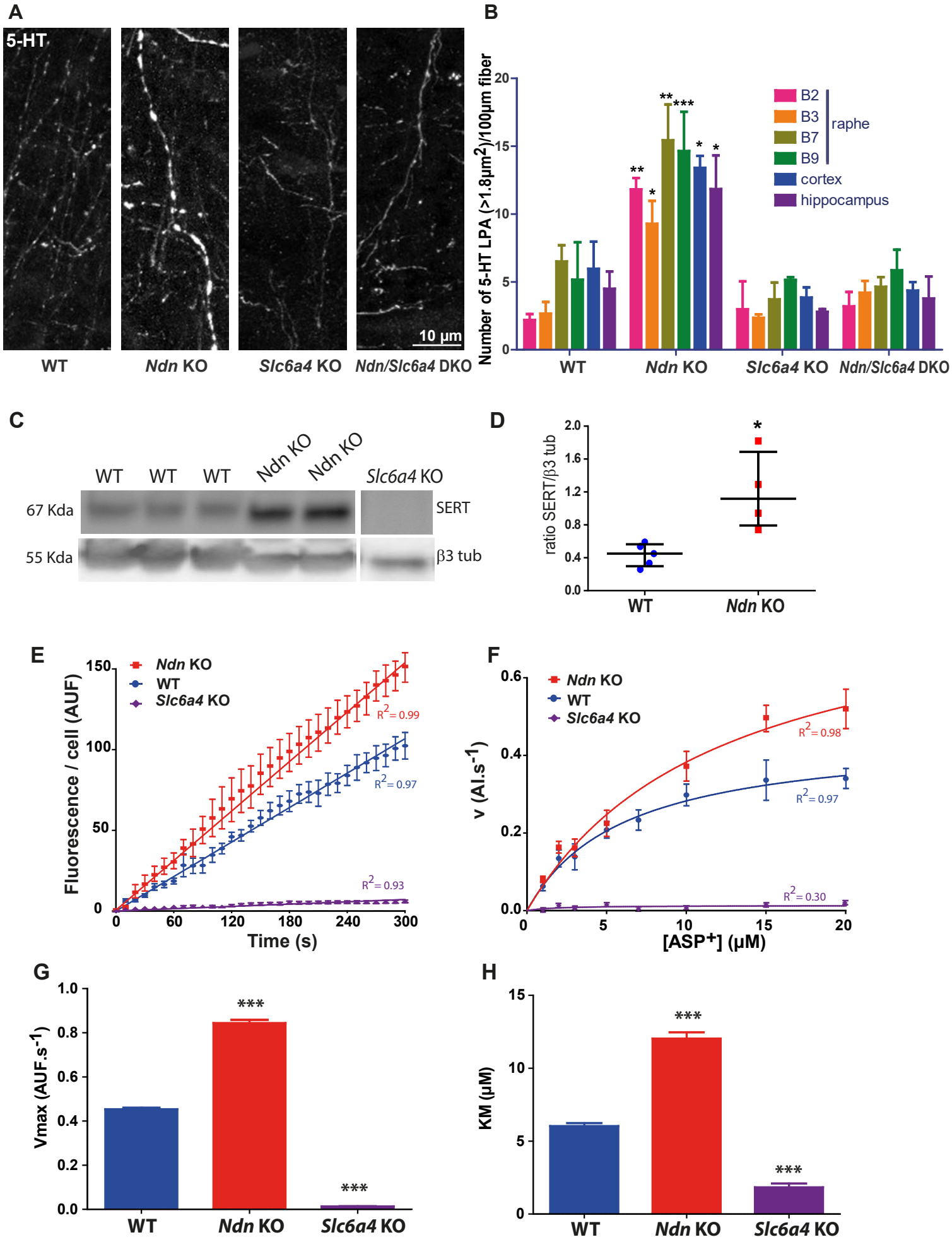
A
5-HT
10 µm
WT
Ndn KO
Slc6a4 KO
Ndn/Slc6a4 DKO
B
Number of 5-HT LPA (>1.8µm²)/100µm fiber
B2
B3
B7
B9
raphe
cortex
hippocampus
C
WT
WT
WT
Ndn KO
Ndn KO
Slc6a4 KO
67 Kda
55 Kda
SERT
β3 tub
D
ratio SERT/β3 tub
E
Ndn KO
WT
Slc6a4 KO
Fluorescence / cell (AUF)
Time (s)
R²= 0.99
R²= 0.97
R²= 0.93
F
v (AI.s⁻¹)
[ASP⁺] (µM)
R²= 0.98
R²= 0.97
R²= 0.30
G
Vmax (AUF.s⁻¹)
H
KM (µM)

FIGURE 2

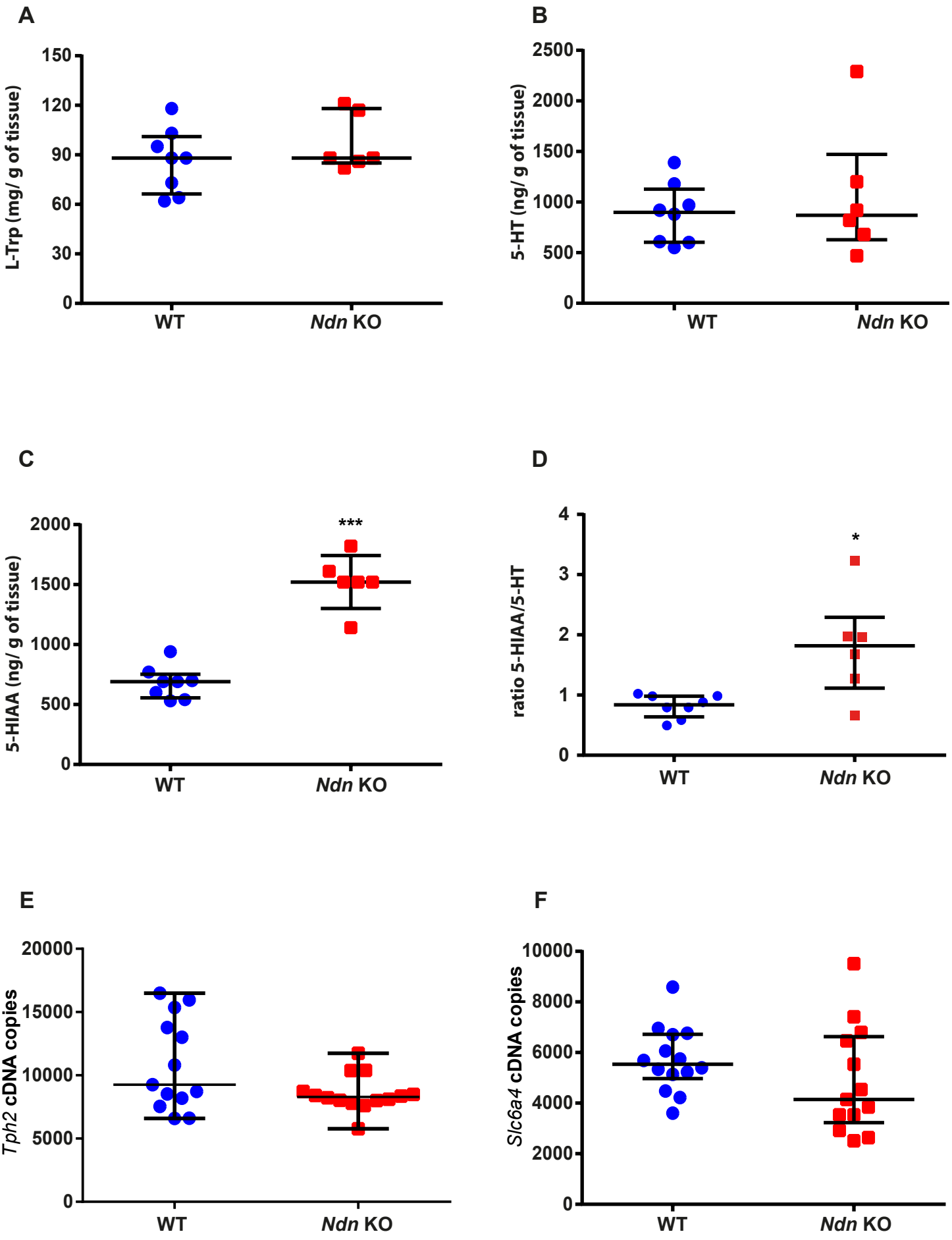

FIGURE 2 - sup 1

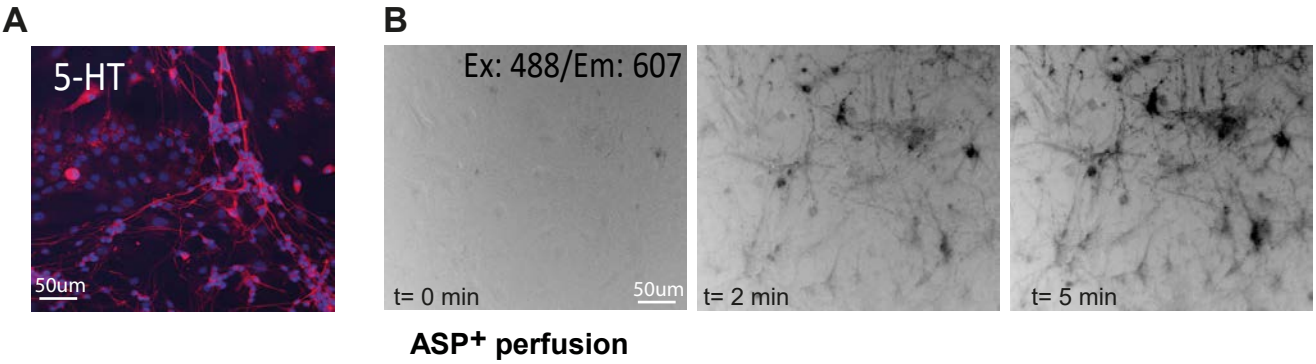

FIGURE 2 - sup 2

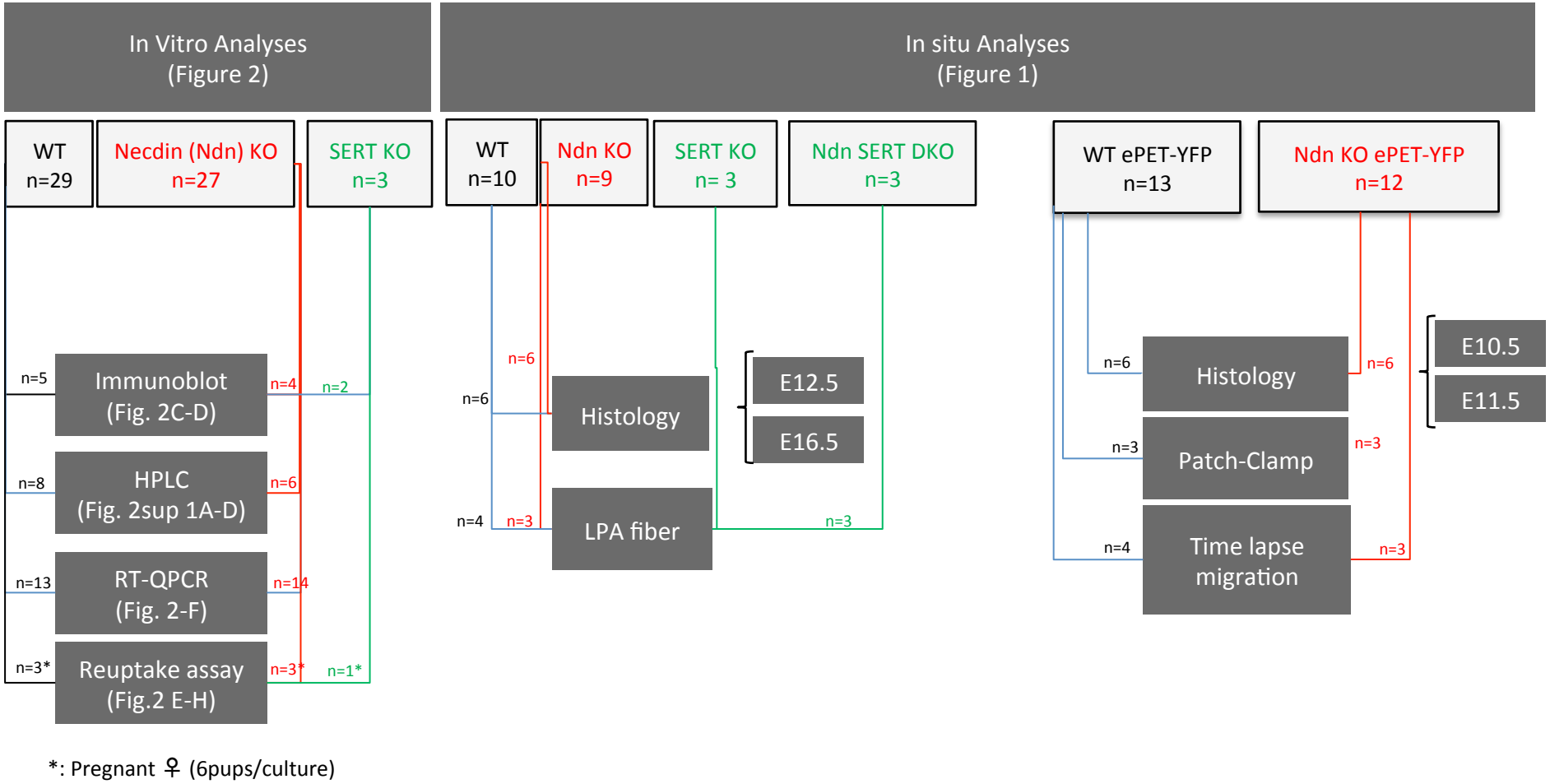

*: Pregnant ♀ (6pups/culture)

Figure 2 sup 3

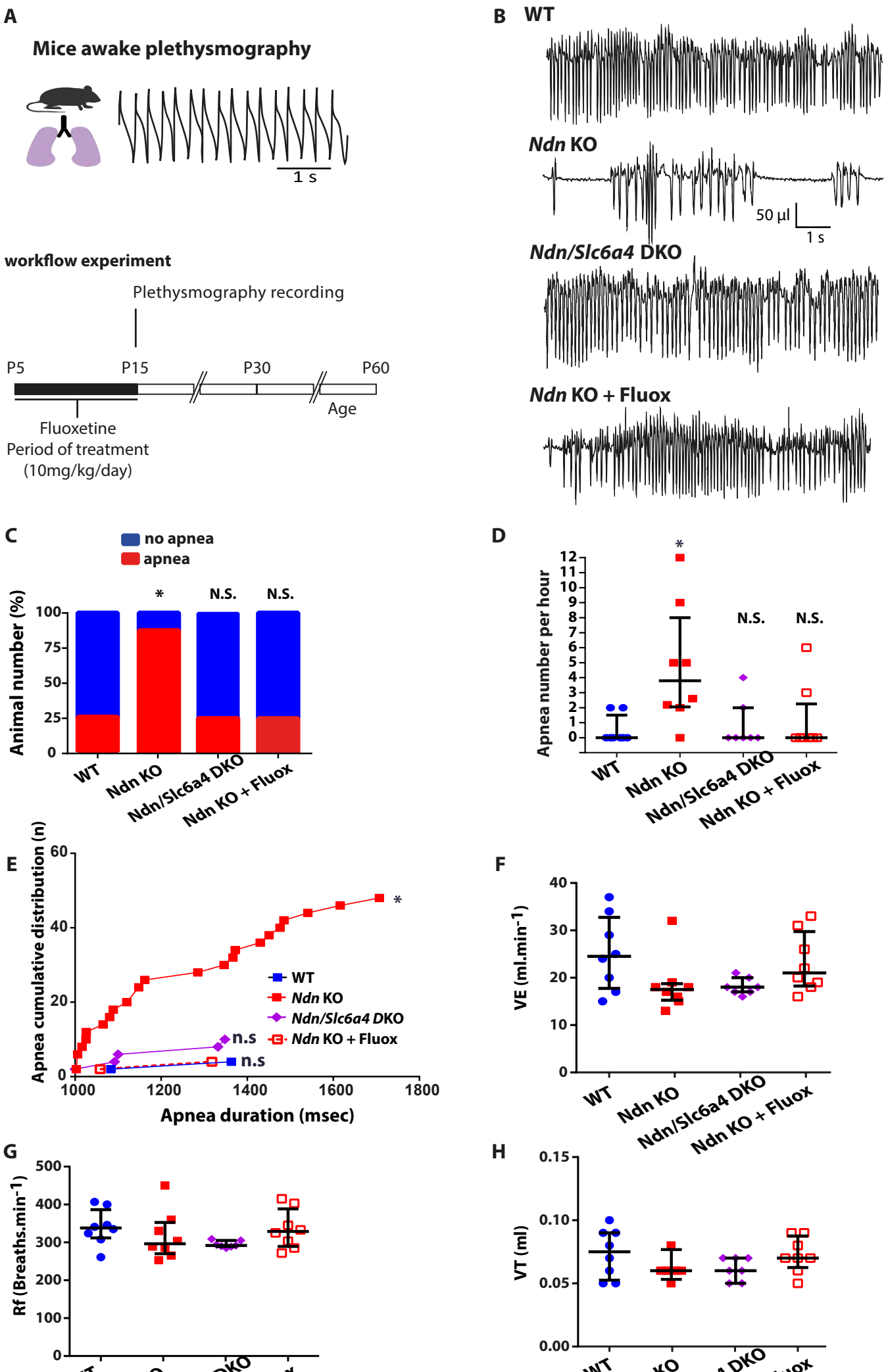
A
Mice awake plethysmography
1 s
workflow experiment
Plethysmography recording
P5
P15
P30
P60
Age
Fluoxetine
Period of treatment
(10mg/kg/day)
B
WT
Ndn KO
50 µl
1 s
Ndn/Slc6a4 DKO
Ndn KO + Fluox
C
no apnea
apnea
Animal number (%)
*
N.S.
N.S.
WT
Ndn KO
Ndn/Slc6a4 DKO
Ndn KO + Fluox
D
Apnea number per hour
*
N.S.
N.S.
E
Apnea cumulative distribution (n)
Apnea duration (msec)
WT
Ndn KO
Ndn/Slc6a4 DKO
Ndn KO + Fluox
n.s
n.s
F
VE (ml.min-1)
G
Rf (Breaths.min-1)
H
VT (ml)

FIGURE 3

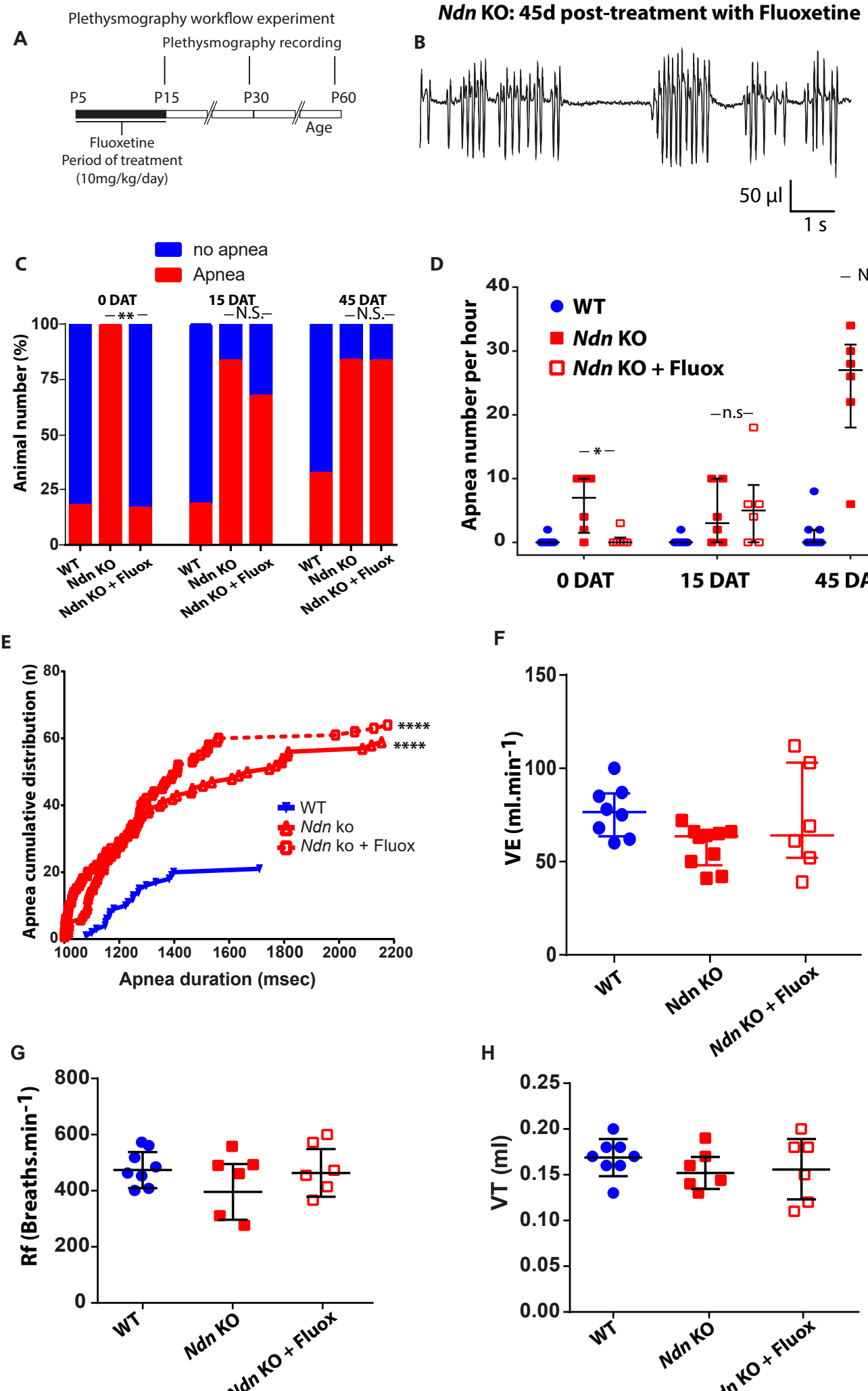

FIGURE 3 Sup 1

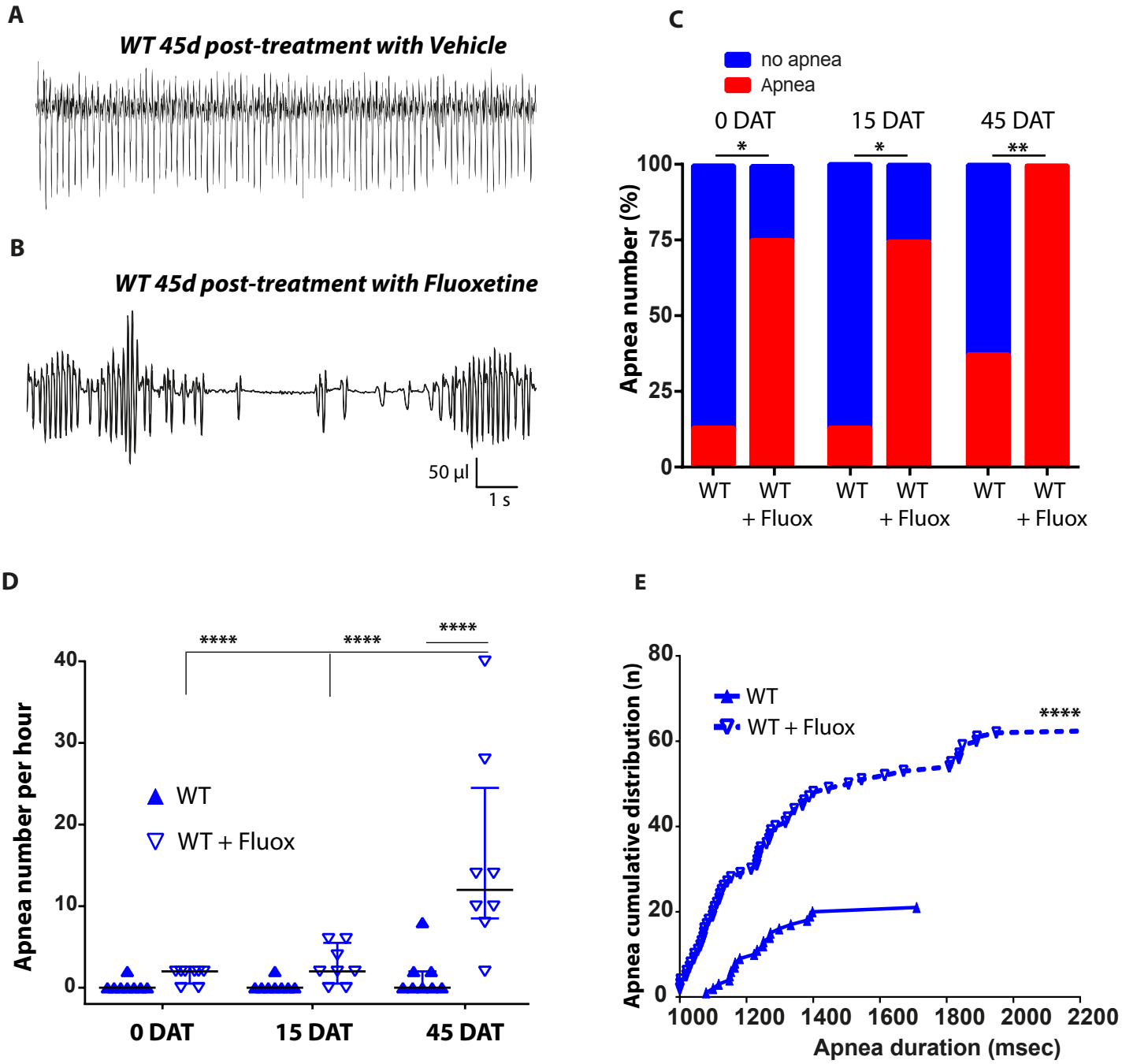

FIGURE 3 - sup 2

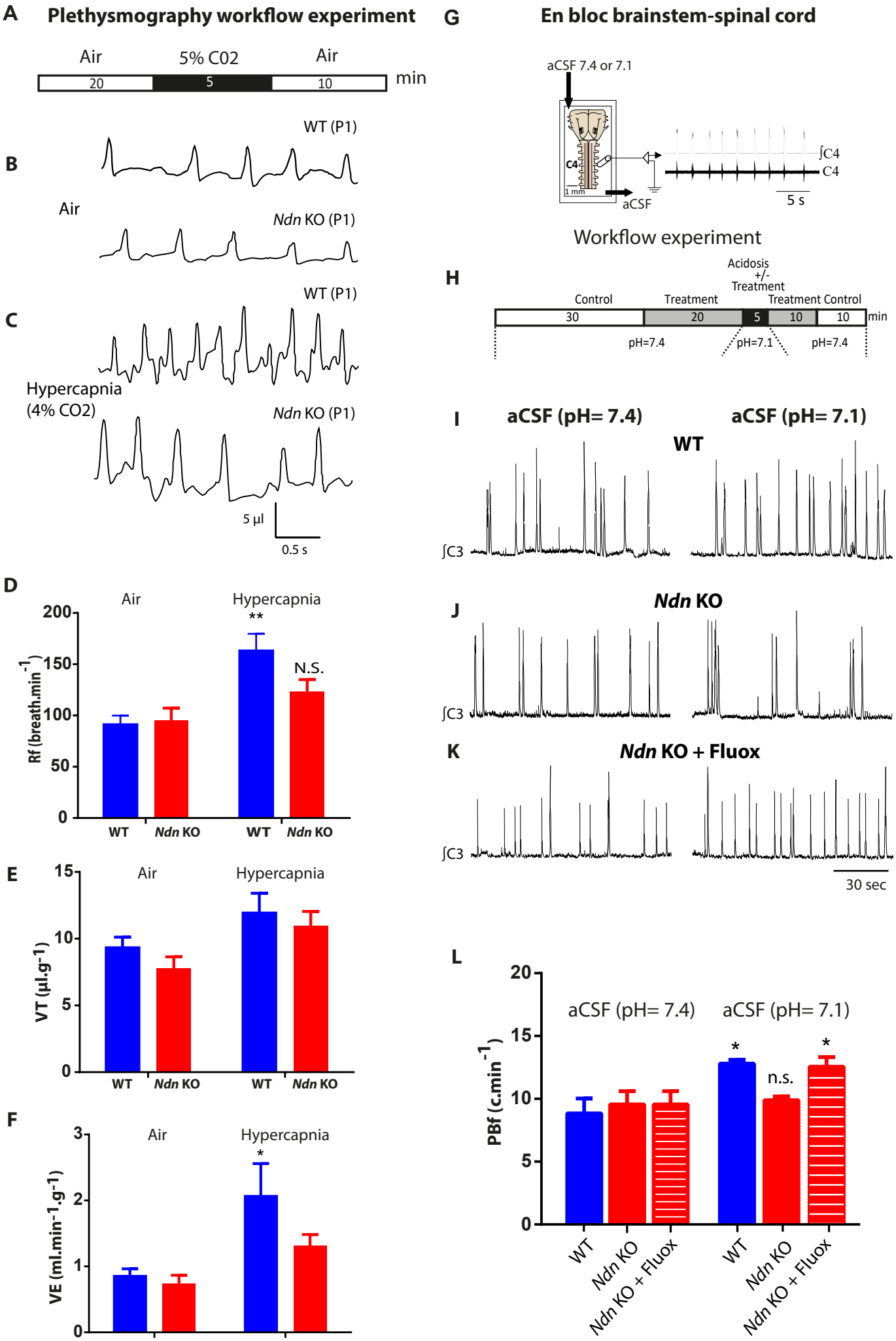
A
Plethysmography workflow experiment
Air
5% C02
Air
20
5
10
min
B
WT (P1)
Air
Ndn KO (P1)
C
WT (P1)
Hypercapnia
(4% CO2)
Ndn KO (P1)
5 µl
0.5 s
D
Air
Hypercapnia
Rf (breath.min-1)
200
150
100
50
0
**
N.S.
WT
Ndn KO
WT
Ndn KO
E
Air
Hypercapnia
VT (µl.g-1)
15
10
5
0
WT
Ndn KO
WT
Ndn KO
F
Air
Hypercapnia
VE (ml.min-1.g-1)
3
2
1
0
*
WT
Ndn KO
WT
Ndn KO
G
En bloc brainstem-spinal cord
aCSF 7.4 or 7.1
C4
1 mm
aCSF
∫C4
C4
5 s
Workflow experiment
H
Acidosis
+/-
Treatment
Control
Treatment
Treatment
Control
30
20
5
10
10
min
pH=7.4
pH=7.1
pH=7.4
I
aCSF (pH= 7.4)
aCSF (pH= 7.1)
WT
∫C3
J
Ndn KO
∫C3
K
Ndn KO + Fluox
∫C3
30 sec
L
aCSF (pH= 7.4)
aCSF (pH= 7.1)
PBf (c.min-1)
20
15
10
5
0
*
n.s.
*
WT
Ndn KO
Ndn KO + Fluox
WT
Ndn KO
Ndn KO + Fluox

FIGURE 4

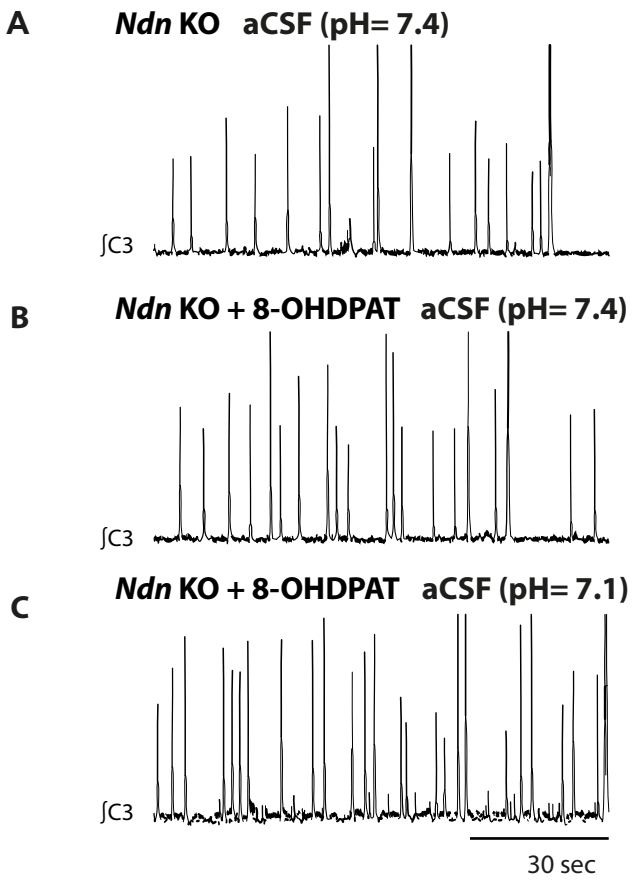

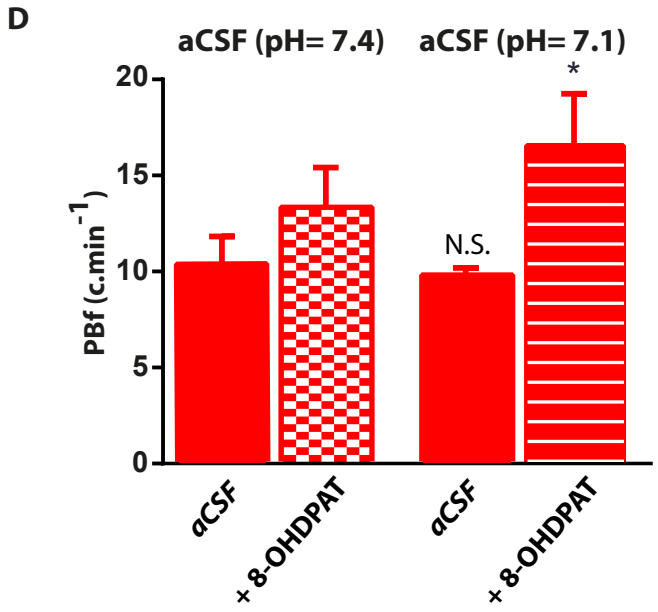

FIGURE 4 sup 1

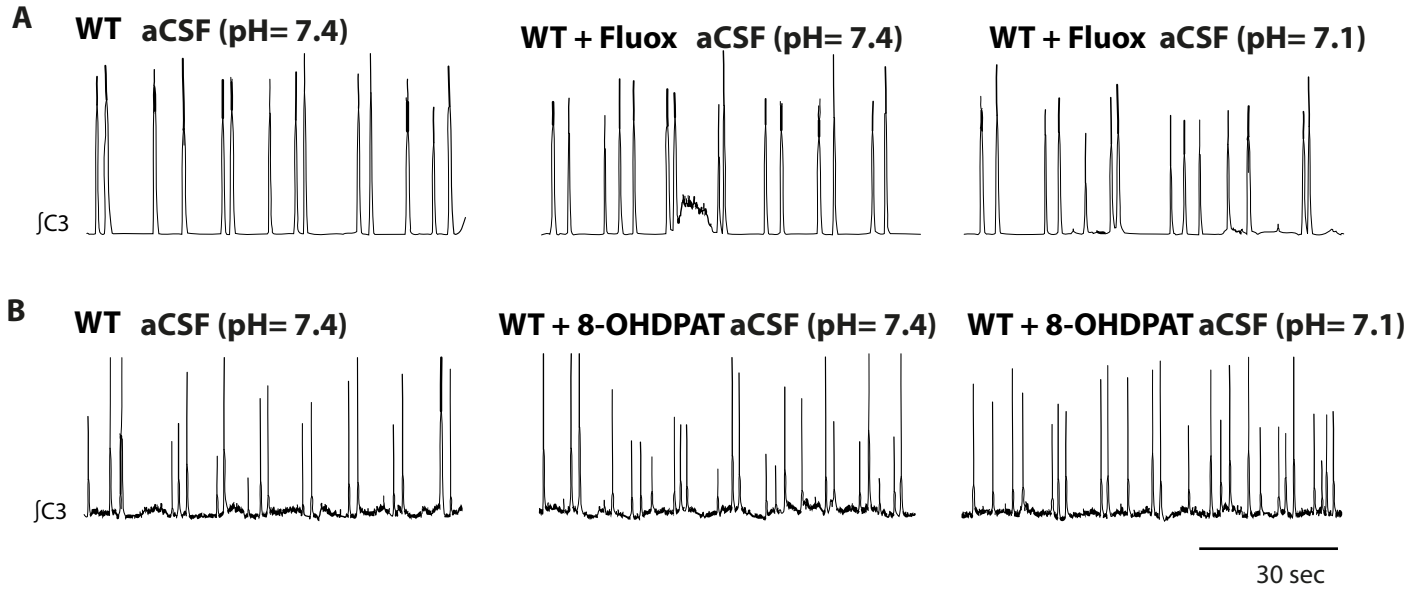

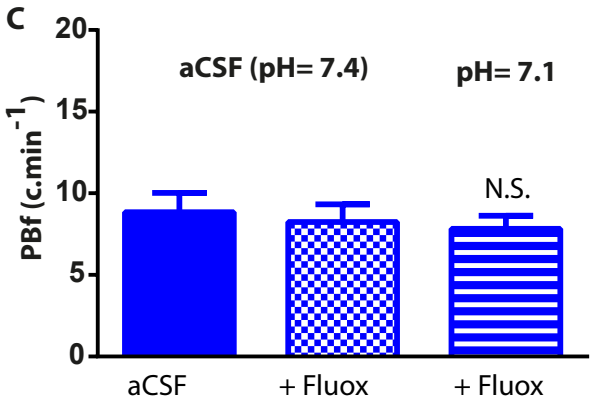

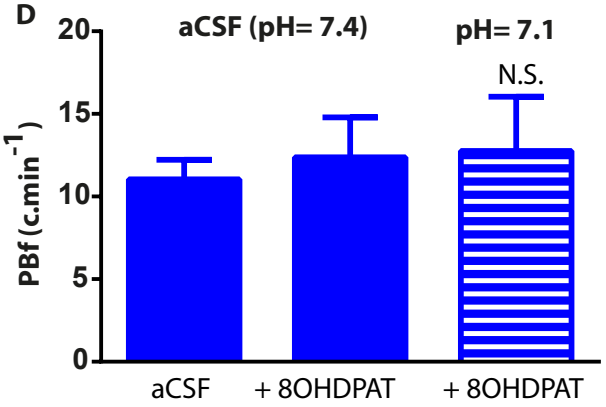

FIGURE 4 sup 2

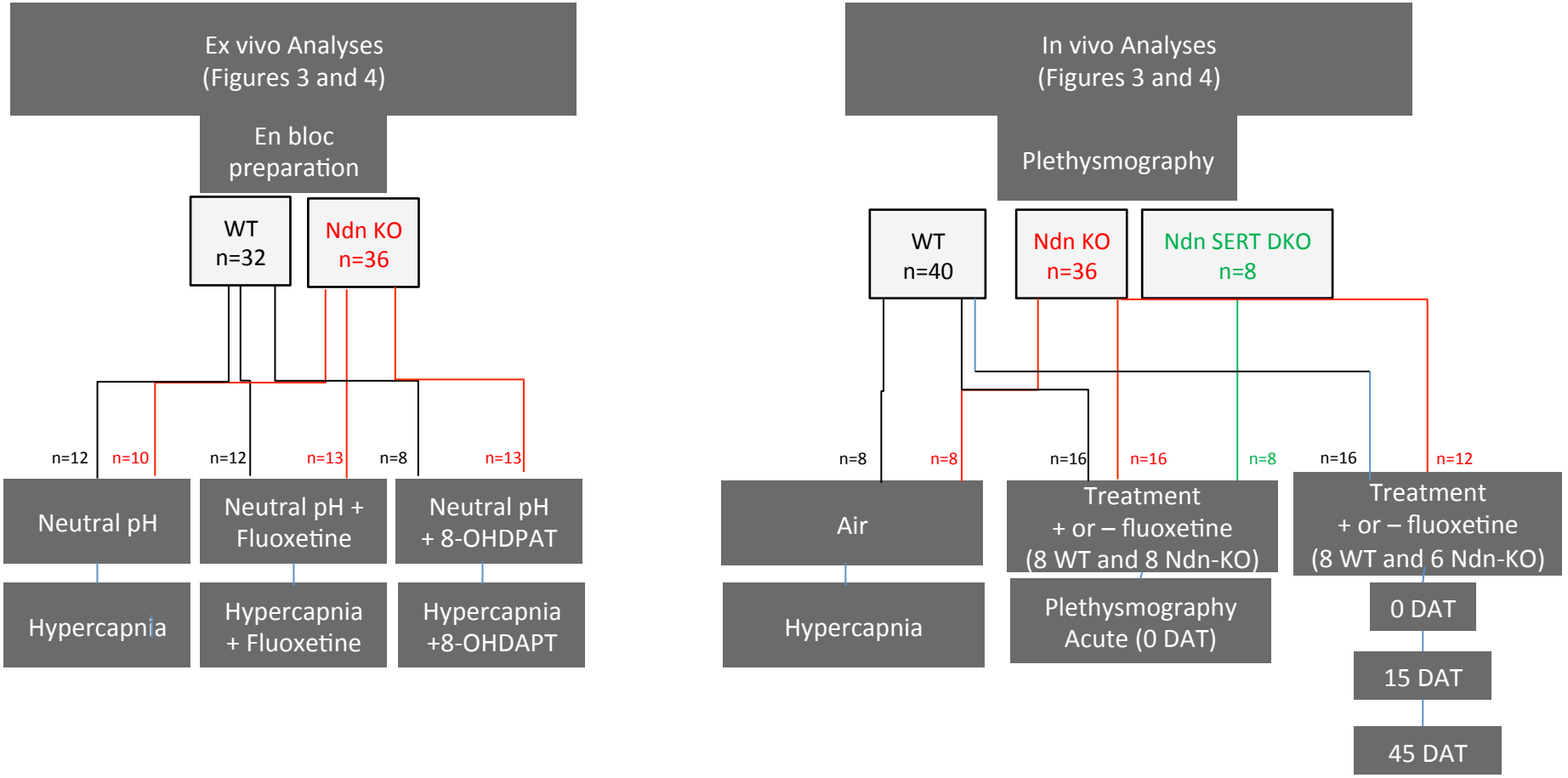

Figure 4 Sup 3